

# The Morphology of Single Chain Asymmetric Block Copolymers in Poor Solvents

Ryan M. Holmes

May 2010



THE AUSTRALIAN NATIONAL UNIVERSITY

An honours thesis submitted for the degree of  
Bachelor of Philosophy in Science

The Australian National University



# Declaration

This thesis is an account of research undertaken between August 2009 and February 2010 at the Department of Applied Maths, Research School of Physics and Engineering, The Australian National University, Canberra, Australia. Except where acknowledged, the material presented in this thesis is, to the best of my knowledge, original and has not been submitted in whole or part for a degree in any university.

---

Ryan M Holmes  
May, 2010



# Acknowledgements

I would like to thank my supervisor David Williams for many informative discussions. Matthew Pinson for his previous work on the subject and for helping me get started. My family for supporting me during the research and my girlfriend.



# Abstract

This thesis investigates the conformations formed by single chain asymmetric block copolymers placed in poor solvents. The investigation is performed using self consistent field theoretic computer simulations developed by the author. A theoretical free energy model of the block copolymer system is also developed. The simulations and free energy model show that the general conformation formed is that of a sphere of the larger species surrounded by various surface domains of the smaller species. The number of these surface domains is predicted by the free energy model and compared to the results of the simulations. The model and simulations are found to agree well for the majority of cases, and best for highly asymmetric polymer chains.

The major impact of this research is a complete understanding of the asymmetric copolymer system. An accurate set of simulations have been carried out and a detailed model which agrees with these simulations has been constructed. These results have direct applications in nano-science, specifically for patchy colloids.



# Contents

<b>Declaration</b>	<b>iii</b>
<b>Acknowledgements</b>	<b>v</b>
<b>Abstract</b>	<b>vii</b>
<b>1 Introduction</b>	<b>1</b>
<b>2 Background Theory</b>	<b>7</b>
2.1 Introduction to Polymer Physics . . . . .	7
2.1.1 The ideal chain . . . . .	7
2.1.2 Real chains . . . . .	10
2.1.3 Block copolymers . . . . .	11
2.2 The Density Field Representation . . . . .	12
2.2.1 Homopolymer volume fraction . . . . .	12
2.2.2 Copolymers . . . . .	14
2.2.3 The mean potential . . . . .	15
2.2.4 The propagator and partition function . . . . .	15
2.2.5 Connecting the propagator and the polymer density . . . . .	17
<b>3 Theoretical Free Energy Models</b>	<b>19</b>
3.1 Preliminary Results . . . . .	20
3.2 Lens Model . . . . .	20
3.2.1 Surface tension . . . . .	22
3.2.2 Chain stretching . . . . .	22
3.2.3 Summary . . . . .	25
3.3 Micelle Model . . . . .	28
3.3.1 Surface tension . . . . .	30
3.3.2 Species <b>A</b> stretching . . . . .	31
3.3.3 Species <b>B</b> stretching . . . . .	31
3.4 Micelle-Lens Comparison . . . . .	31

<b>4 Self Consistent Field Theory Implementation and Method</b>	<b>35</b>
4.1 Simulation Process . . . . .	37
4.1.1 Initialization . . . . .	37
4.1.2 Iterative loop . . . . .	37
4.2 Solving the Propagator Equation . . . . .	40
4.3 Free Energy Calculation . . . . .	41
4.3.1 Simple simulation check . . . . .	42
4.4 Simulation Stability . . . . .	43
4.4.1 $\Delta\phi$ term . . . . .	43
4.4.2 Other optimizations . . . . .	45
<b>5 Results and Analysis</b>	<b>47</b>
5.1 Convergence Range . . . . .	47
5.2 Reproducibility . . . . .	49
5.3 General Conformation Trends . . . . .	49
5.3.1 Larger species centralized . . . . .	49
5.3.2 Parameter trends . . . . .	50
5.4 Comparison to the Lens Model . . . . .	52
5.5 Result Validity . . . . .	56
5.6 Model Comparison (Valid Conformations Only) . . . . .	58
5.7 Possible Solutions to the Statistical Problem . . . . .	60
5.7.1 Hard sphere . . . . .	60
5.7.2 A block interaction . . . . .	61
<b>6 Conclusion and Summary</b>	<b>63</b>
6.1 Further Directions . . . . .	65
6.2 Outcome Summary . . . . .	65
<b>Bibliography</b>	<b>70</b>
<b>7 Appendix 1: The Solution to the Propagator Equation</b>	<b>71</b>
7.1 Mean Field Formula . . . . .	71
7.2 Solving the Propagator Equation . . . . .	72
7.2.1 Finding the coefficients using the Wilcox method . . . . .	73
7.2.2 Solution in terms of separated exponentials . . . . .	77
7.2.3 Solution of simple diffusion equation . . . . .	78
7.2.4 Final solution . . . . .	80
<b>8 Appendix 2: Free Energy Model Calculations</b>	<b>81</b>
8.1 Lens Model Calculations . . . . .	81
8.1.1 Surface tension . . . . .	82

8.1.2	Species <b>B</b> stretching . . . . .	82
8.1.3	Species <b>A</b> stretching . . . . .	85
8.1.4	Relating $k$ to $x$ . . . . .	86
8.2	Micelle Model Calculations . . . . .	86
8.2.1	Surface tension . . . . .	86
8.2.2	Species <b>B</b> stretching . . . . .	87



# Chapter 1

## Introduction

### Polymers

Polymers form a diverse range of materials and draw interest from a variety of fields. Synthetic polymers have many applications as useful materials in plastics, clothing and rubber [30]. Polymers have the potential to be used in nano-science due to their ability to self assemble into nanometer scale structures [24, 29, 34]. A large range of polymers exist inside living matter as structures such as DNA, RNA and proteins. These biological polymers are the subject of much modern research in existing unsolved problems such as protein folding [5, 4].

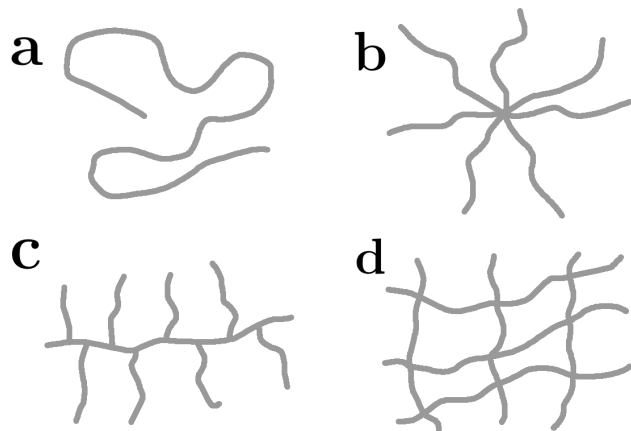


Figure 1.1: Different polymer architectures: a) linear, b) star, c) bottle brush and d) network.

A polymer consists of a long chain of repeating structural units called *monomers*. The chain can have a range of different architectures, from a simple linear chain

to the star, bottle brush, and polymer networks shown in figure 1.1.

Each monomer in the chain is typically made up of one or many molecules, such as an ethylene molecule ( $C_2H_4$ ) in the case of polyethylene. A *homopolymer* is a polymer that only has one species of monomer while a *copolymer* (or heteropolymer) consists of two (or more) monomer species. The different monomer species can be arranged randomly along the chain or, in the case of a *block copolymer*, the monomer species form repeating blocks (figure 1.2).



Figure 1.2: (left) A homopolymer and (right) a block copolymer containing blocks of monomer types **A** and **B**.

Polymers are often dissolved in a solvent. The solvent consists of a large number of smaller particles such as water molecules. The quality of the solvent is a measure of how much the polymer prefers contact with the solvent as opposed to itself. In a *good solvent* the polymer prefers being in contact with the solvent and hence swells to increase solvent surface contact. In a *poor solvent* the polymer tends to collapse into a more compact globule to minimize solvent surface contact.

### Single chain block copolymers

This thesis investigates the properties of *flexible single block copolymer chains in poor solvents* where the blocks of each species (**A** and **B**) have a constant number of monomers. The polymer can form a large range of *conformational shapes* (referred to as conformations) due to the interplay of a variety of effects. Overall, the polymer prefers to form a compact spherical globule to minimize contact with the solvent. In addition, the **A** and **B** portions of the polymer prefer to phase separate and form individual domains to minimize **A-B** surface contact. However, the polymer must also stay connected and the chain pays a high free energy penalty for stretching. This stretching effect frustrates the formation of two simple **A** and **B** domains inside a spherical globule. Instead the conformations formed are typically highly contorted and are fragmented into many separate domains.

The main focus in this work is on *asymmetric single block copolymer chains in poor solvents*, where the blocks of species **A** contain significantly less monomers

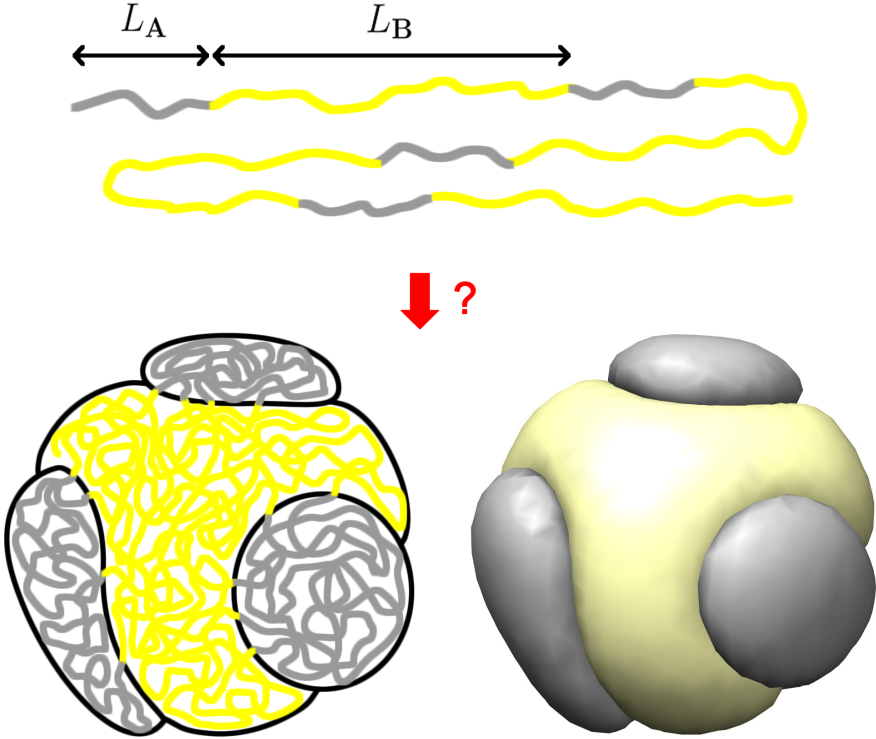


Figure 1.3: (upper drawing) An asymmetric single copolymer chain. The amount of asymmetry is measured by the block size ratio  $\mathcal{R} = \frac{N_A}{N_B} = \frac{L_A}{L_B}$ . When placed in a poor solvent, this polymer chain will collapse to form a compact globule with some conformation (lower drawing and corresponding SCFT simulation image). This thesis attempts to predict what conformations will be formed by various polymer chain configurations and explain why these conformations are formed.

than the species **B** blocks (figure 1.3). The block size ratio  $\mathcal{R} = \frac{N_A}{N_B}$ , where  $N_A$  and  $N_B$  are the number of monomers of species **A** and **B**, is an important factor in determining the conformation into which the polymer collapses. Typically, as the length of the **A** blocks gets smaller, the **A** species forms a number of separate domains on the surface of an approximately spherical **B** domain. This thesis attempts to explain the formation of this conformation and to predict the number of surface **A** domains for a range of different conditions. The investigation involves several different approaches. A theoretical free energy model is developed using simple surface tension and stretching free energy terms. This model is compared to the results of computer simulations performed on the system using *self consistent field theory* (SCFT) [10, 19].

## Previous work and applications

Most modern research in polymer physics focuses on *polymer melts* which contain *many* single polymer chains together without a solvent [19, 18, 22]. Polymer melts have a fundamentally different structure to single polymer chains as the domains formed contain parts of many different polymer chains. Clearly, the study of polymer melts is of great importance to the materials industry and most research focuses there, rather than on single polymer chains in dilute solutions. Consequently, our understanding of polymer melts is more extensive than our understanding of the more fundamental object of a single polymer chain. The case of single chains is important from a theoretical point of view. It is also of interest in biology in studies of the protein folding problem and in genetics and DNA studies [5, 4, 23]. Single chain copolymers have possible applications as separate structured nano-particles [24, 29, 34], and patchy colloids [36]. In addition, there have been proposals to make microscopic memory devices from single polymer chains [14].

The possibility of forming patchy colloid like particles from block copolymers is particularly interesting. Patchy colloids are micrometer diameter size particles which have a number of special *sticky patches* on their surface. These patches give the colloidal particles interesting structural properties, such as the ability to self-assemble into intricate structures. The work in this thesis indicates that there could be the potential to form similar patchy particles from block copolymers. If formed from block copolymers the patchy particles would have a smaller scale than normal colloidal particles, being of the order of 10's of nanometers.

Most previous research on *single polymer chains* has focused on the simple homopolymer case, investigating aspects such as single chain stretching [12, 1]. The homopolymer case is now well understood [38], but the more complex copolymer case has not been investigated thoroughly either theoretically or with simulations. Some work has been done using monte carlo and molecular dynamics simulations on *symmetric* block copolymers where the blocks of each species have the same length [25]. Recently this symmetric case has also been investigated using SCFT simulations [27]. This work has given a general understanding of the overall conformation formed by single chain symmetric block copolymers in poor solvents. However, little work has been done on the conformations of *asymmetric* block copolymers in poor solvents where the blocks of each species have different lengths. This is the subject of this thesis.

## Thesis outline

Chapter two gives an introduction to polymer physics, summarizing the important ideas in the field. Concepts and formulas required for the subsequent chapters are

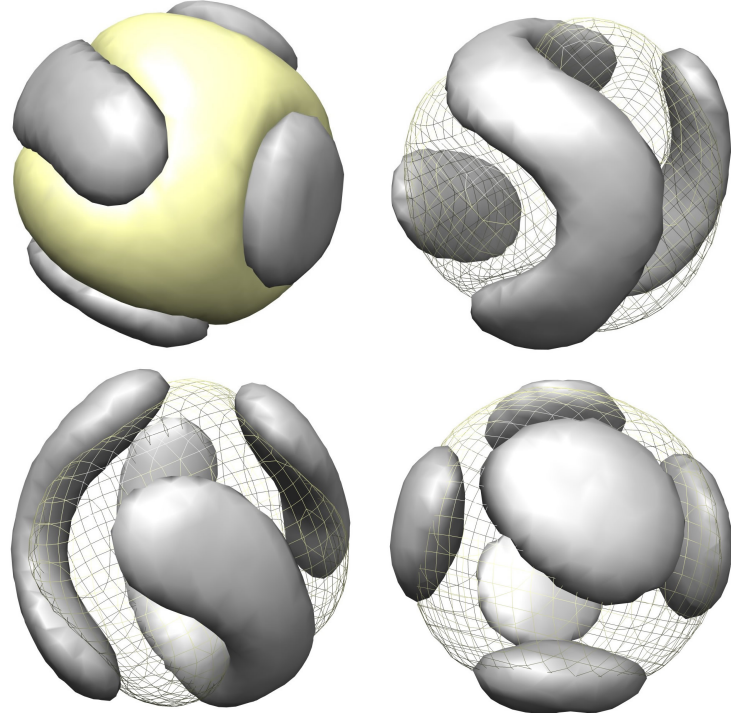


Figure 1.4: Example copolymer conformations produced using the self consistent field theory simulations.

outlined. The density field representation of a polymer on a lattice is introduced along with the fundamental statistical quantity required for the simulations, the propagator.

Chapter three develops a theoretical free energy model for the polymer systems considered. The findings of this model are investigated and compared to an inverse conformation model to explain the general conformation characteristics.

Chapter four outlines the SCFT simulation method including the relevant mathematical basis. The method for solving the propagator equation is described as well as the overall simulation process. Optimizations of the code are described briefly.

Chapter five presents the results of the computer simulations and discusses the general conformation trends. The simulation results are compared to the theoretical model and an understanding of the polymer system is developed.

Chapter six concludes and reviews the work.

The derivation of the mathematical solution to the propagator equation is presented in appendix one. Appendix two includes some of the calculations for the free energy models considered in chapter three.



# Chapter 2

## Background Theory

This chapter gives an overview of the physics of polymers, focusing mainly on concepts and formulas required for subsequent chapters. An understanding of the basic stretching and surface tension interactions existing in polymer systems is vital if an accurate theoretical model is to be developed.

An overview of the *density field representation* of a polymer on a lattice is given. This forms the mathematical basis from which the self consistent field theory simulation method is derived.

### 2.1 Introduction to Polymer Physics

#### 2.1.1 The ideal chain

The simplest way to describe a polymer chain is as an *ideal chain*. In an ideal chain there are no interactions between the repeating structural units (monomers) along the chain and hence the polymer acts as a *random walk* in space (figure 2.1). A random walk is generated by starting at a particular point and randomly choosing the direction in which to place the next segment. This completely random process is repeated for each segment along the chain. Consequently, the segments are uncorrelated with each other.

If the segment vectors between consecutive monomers are given by  $\mathbf{b}_1, \mathbf{b}_2 \dots \mathbf{b}_N$  and the segment length (or monomer size) is  $b$ , then the *mean square end-to-end*

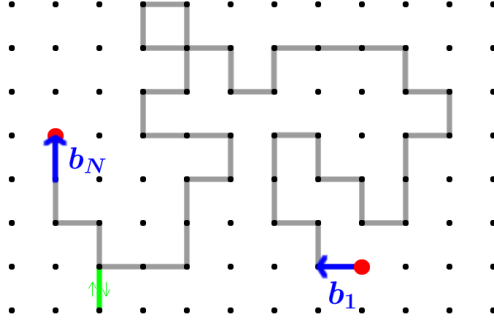


Figure 2.1: A random walk on a lattice. The starting and ending points are indicated in red and the bond vectors  $b_1$  and  $b_N$  in blue. The chain can turn back on itself (green segments), as there are no correlations between consecutive segments.

distance  $R_0$  of the ideal chain is given by:

$$\begin{aligned} R_0^2 &= \left\langle \left| \sum_{n=1}^N \mathbf{b}_n \right|^2 \right\rangle \\ &= \left\langle \sum_{n=1, m=1}^N \mathbf{b}_n \cdot \mathbf{b}_m \right\rangle \end{aligned}$$

As there are no interactions or correlations between different segments along the chain, only the diagonal terms of the average are included so:

$$R_0^2 = \left\langle \sum_{n=1}^N |\mathbf{b}_n|^2 \right\rangle = Nb^2 \quad (2.1)$$

This average square end-to-end distance gives a measure of the natural size of an ideal chain.

### Stretching an ideal chain

For long ideal chains where  $N$  is large, the end-to-end vector  $\mathbf{R} = \mathbf{r}_N - \mathbf{r}_0$  obeys a gaussian probability distribution [6]:

$$P(\mathbf{R}) = \left( \frac{3}{2\pi Nb^2} \right)^{3/2} \exp \left( -\frac{3\mathbf{R}^2}{2Nb^2} \right)$$

Given this distribution, the entropy of the ideal chain given a particular end-to-end length  $R$  is [15]:

$$\begin{aligned} S(R) &= k_B \ln (P(\mathbf{R})) \\ &= -\frac{3k_B R^2}{2R_0^2} \end{aligned}$$

The *Helmholtz free energy* associated with a particular elongation length  $R$  can be found given  $F = E - TS$ . The free energy is an important quantity in polymer physics. The polymer will form the conformation that has the minimum free energy.

For the ideal chain case there are no interactions so the energy  $E$  is a constant. So up to an additive constant:

$$F(R) = \frac{3k_B T}{2} \frac{R^2}{R_0^2} \quad (2.2)$$

This formula shows that when stretched, an ideal chain acts as a simple spring with spring constant  $\frac{3k_B T}{R_0^2}$ . This formula is used in the theoretical free energy model to quantify linear stretching within the collapsed polymer conformations.

### Crushing an ideal chain

The scaling of the free energy of an ideal chain crushed into a sphere of radius  $R$  can be found by the following argument.

Due to the absence of interactions, the polymer chain will perform a random walk except when it comes close to the sphere wall. The chain is then restricted to move away from the wall, halving the possible angle space of motion. Each collision with the wall results in a free energy loss on the order of  $k_B T$ . The total free energy loss is then  $k_B T$  times the number of wall collisions  $\mathcal{C}$ :

$$F \propto k_B T \times \mathcal{C}$$

The polymer chain will random walk across the sphere in-between each collision with the wall. The number of monomers  $N_s$  in each random walk segment between collisions can be calculated:

$$\begin{aligned} R_0 &\approx 2R \\ \implies \sqrt{N_s b^2} &\approx 2R \\ \implies N_s &\approx \frac{4R^2}{b^2} \end{aligned}$$

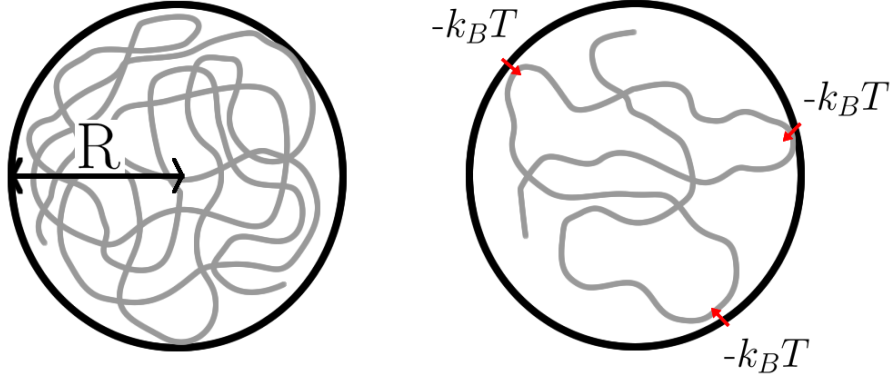


Figure 2.2: An ideal polymer chain crushed into a sphere. The chain loses  $\propto k_B T$  free energy in each collision with the sphere wall. In-between collisions the chain performs a random walk of monomer length  $N_s$ .

If there are  $N$  total monomers, then the number of random walk segments, equivalent to the number of collisions  $\mathcal{C}$  is:

$$\mathcal{C} \propto \frac{N}{N_s} \propto \frac{Nb^2}{R^2}$$

So the free energy of an ideal chain crushed into a sphere of radius  $R$  is:

$$F \propto k_B T \frac{R_0^2}{R^2} \quad (2.3)$$

This formula will be used in section 4.3 as a simple check of the simulation method.

### 2.1.2 Real chains

In real polymer chains there are long range interactions between monomers which are not necessarily adjacent along the chain (figure 2.3). In an ideal chain two monomers can exist in the same position (figure 2.1). In real chains this is clearly not possible. This kind of interaction is termed *steric repulsion*. There are also *attractive* Van der Walls forces between different monomers. The balance of these attractive and repulsive forces determines whether the real polymer tends to swell or contract relative to the ideal chain size. [17]

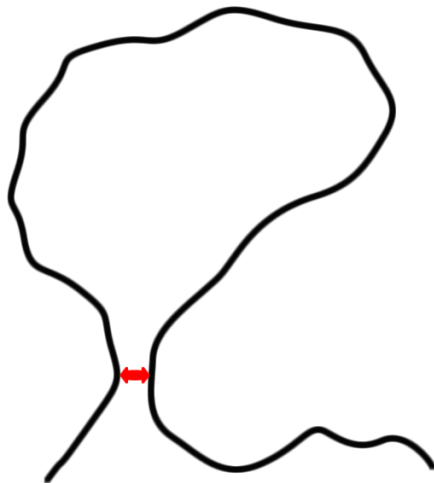


Figure 2.3: A long range interaction existing in real chains and not in ideal chains.

Polymers are often dissolved in a solvent. The presence of the solvent heavily influences the balance between attractive and repulsive long-range interactions. The quality of the solvent can be described by the *Flory interaction parameter*  $\chi$ .  $\chi < \frac{1}{2}$  is the good solvent regime, where the balance of interactions is such that the polymer tends to swell from its ideal size.  $\chi > \frac{1}{2}$  is the poor solvent regime, where the polymer tends to collapse into a compact globule. The point  $\chi = \frac{1}{2}$  is termed the *theta point* and corresponds to a cancelation between the attractive and repulsive long-range interactions. A polymer in a *theta solvent* acts almost as an ideal chain. [3]

In this thesis only polymers in poor solvents are considered. Here the polymer will collapse into a spherical globule with a density dependent on the solvent quality  $\chi$ . The resulting density is an important factor affecting the collapsed conformation. The density can be determined by minimizing the free energy (section 2.2.1).

### 2.1.3 Block copolymers

When blocks of a second species of polymer are introduced to the chain, additional interactions become significant. There will be an interaction and hence a Flory interaction parameter  $\chi_{AB}$  between the two polymer species **A** and **B**. For the case of interest where the polymer species form separate domains, this parameter will be positive, indicating repulsion. The strength of the **A-B** interaction influences the end conformation of the copolymer as a larger  $\chi_{AB}$  will favor less contact

between the two species.

It is possible that the two species have different interaction strengths with the solvent. This can cause interesting conformations where one species surrounds the other, to minimize the inner species surface contact with the solvent. This case is not considered in this thesis and the interaction strength between both species and the solvent is taken as  $\chi$ .

## 2.2 The Density Field Representation

Polymer conformations can be represented by a *density field on a lattice*. This is an important concept and is used throughout this thesis in both the theoretical model and the computer simulations.

In the case of a *homopolymer and a solvent*, the polymer is described by a density  $\phi$  at every point in space (lattice site). This density is normalized to 1 and hence it is also termed the *volume fraction* of polymer. This implies that the volume fraction of solvent at each site is  $\phi_S = 1 - \phi$ . The free energy associated with a polymer density field system on a lattice has several contributions (units of  $k_B T$  are adopted throughout):

- *Configurational entropy of the polymer*, described by the partition function  $\mathcal{Z}$ . This is the entropy a polymer has by virtue of its random shape (figure 2.4). The term is evaluated by introducing a statistical function called the *propagator* that ensures the density field describes a connected polymer chain. See section 2.2.4.
- *Polymer-solvent interaction energy*, described by the interaction parameter  $\chi$ . This term is simply given by the overlap between  $\phi$  and  $\phi_S$  times  $\chi$  for each lattice site:

$$F_{PS}|_{\text{site}} = \chi\phi(1 - \phi)$$

- *Translational entropy of the solvent* given by [38]:

$$F_S|_{\text{site}} = \phi_S \log \phi_S = (1 - \phi) \log (1 - \phi)$$

The total free energy is the sum of these terms.

### 2.2.1 Homopolymer volume fraction

A homopolymer in a poor solvent will collapse to form a sphere with some polymer volume fraction  $\phi$ .  $\phi$  will be such that the total free energy is minimized. The configurational entropy term does not depend directly on  $\phi$  and hence can be ignored for this exercise.

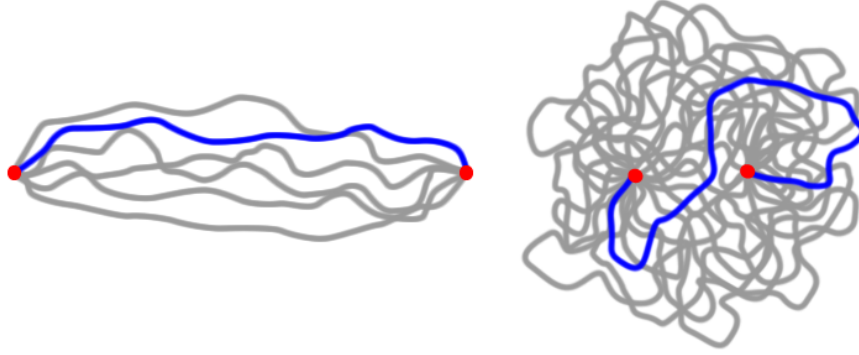


Figure 2.4: A stretched polymer chain (left) has less possible chain arrangements than a free polymer chain (right). The stretched chain has a lower *configurational entropy* and hence a higher free energy relative to the free polymer chain. Single possible chain arrangements are highlighted in blue.

If  $\phi$  at a particular site is equal to 1 then the volume associated with that point is set to be a monomer volume  $v = \frac{4}{3}\pi b^3$ . If the polymer contains  $N$  monomers and forms a sphere of radius  $R$ , then since  $\phi$  is the volume fraction of polymer, by volume conservation:

$$\frac{4}{3}\pi R^3\phi = vN \implies R^3 = \frac{b^3 N}{\phi} \quad (2.4)$$

Hence the number of sites taken up by the polymer is given by:

$$\text{sites} = \frac{\frac{4}{3}\pi R^3}{v} = \frac{N}{\phi}$$

And the free energy is:

$$\begin{aligned} F &= \left( \chi\phi(1 - \phi) + (1 - \phi) \log(1 - \phi) \right) \frac{N}{\phi} \\ &= \chi(1 - \phi)N + \left( \frac{1}{\phi} - 1 \right) \log(1 - \phi)N \end{aligned}$$

Taking the derivative w.r.t  $\phi$  and setting to zero to minimize the free energy gives:

$$\begin{aligned} \chi + \frac{1}{\phi^2} \log(1 - \phi) + \left( \frac{1}{\phi} - 1 \right) \frac{1}{1 - \phi} &= 0 \\ \implies \chi\phi^2 + \phi + \log(1 - \phi) &= 0 \end{aligned}$$

Assuming a linear approximation to this equation (figure 2.5) between the values of  $\chi = 0.6$  and  $\chi = 0.8$  gives the density of polymer within the sphere:

$$\phi = 1.4(\chi - 0.42) \quad (2.5)$$

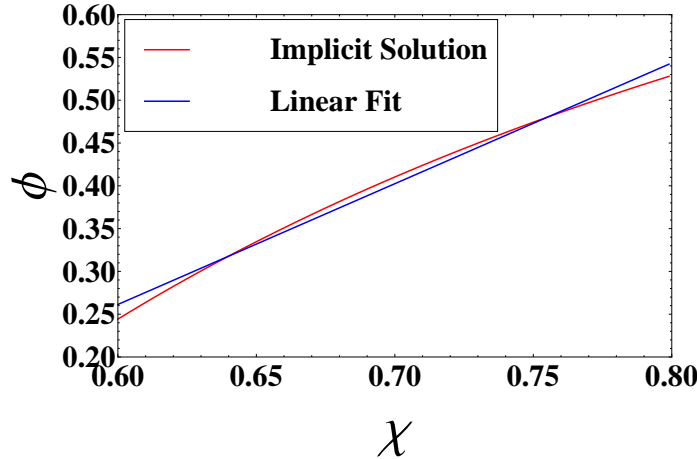


Figure 2.5:  $\phi = 1.4(\chi - 0.42)$  linear approximation to the solution of  $\chi\phi^2 + \phi + \log(1 - \phi) = 0$  within the range  $0.6 < \chi < 0.8$ .

The range of  $\chi$  values is between 0.6 and 0.8 as these are physically reasonable poor solvent values. For  $\chi$  values below 0.6 the solvent becomes too much like a good solvent and the low density of polymer causes problems in the simulations. Similarly, for high  $\chi$  the density of polymer gets too high and causes errors. (see section 5.1)

### 2.2.2 Copolymers

When a second polymer species is introduced there are two density fields  $\phi_A$  and  $\phi_B$  describing the two species, so the density of the solvent is  $\phi_S = 1 - \phi_A - \phi_B$ . The only additional free energy term is that of the interaction between species **A** and **B**, which is of the same form as the polymer-solvent interaction:

$$F_{AB}|_{\text{site}} = \chi_{AB}\phi_A\phi_B$$

The polymer-solvent term is also split into an **A** interaction and a **B** interaction ( $\phi\chi = (\phi_A + \phi_B)\chi$ ). The total free energy is given by:

$$F = -\log \mathcal{Z} + \int_V [\phi_S \log(\phi_S) + \chi(\phi_A\phi_S + \phi_B\phi_S) + \chi_{AB}\phi_A\phi_B] d\mathbf{r} \quad (2.6)$$

Where the integral is over all lattice sites. The polymer will settle into the conformation with the lowest free energy. So at equilibrium  $\frac{\partial F}{\partial \phi_A}$  and  $\frac{\partial F}{\partial \phi_B}$  will be equal to 0.

### 2.2.3 The mean potential

The task of the computer simulation method is to find the density fields  $\phi_A$  and  $\phi_B$  such that the above expression for the free energy is minimized. In order to make this problem tractable, a *mean potential* is introduced. As monomers of the two different species have different interactions, there will be a mean potential felt by an **A** monomer  $w_A$  and a mean potential felt by a **B** monomer  $w_B$ . These mean potentials are introduced into the free energy formula (2.6) in the form of additional terms:

$$F_w = - \int_V w_A \phi_A + w_B \phi_B d\mathbf{r}$$

Given polymer densities  $\phi_A$  and  $\phi_B$ , the forms of  $w_A$  and  $w_B$  can be found by carrying out the minimization of the free energy with respect to  $\phi_A$  and  $\phi_B$ . This gives (see appendix 1 for derivation):

$$w_A(\mathbf{r}) = \chi(1 - 2\phi_A - 2\phi_B) + \chi_{AB}\phi_B - \log(1 - \phi_A - \phi_B) \quad (2.7)$$

and

$$w_B(\mathbf{r}) = \chi(1 - 2\phi_A - 2\phi_B) + \chi_{AB}\phi_A - \log(1 - \phi_A - \phi_B) \quad (2.8)$$

### 2.2.4 The propagator and partition function

General density fields  $\phi_A$  and  $\phi_B$  do not necessarily describe a *connected polymer chain*. To return the connected polymeric nature to the density field, the statistical partition function and propagator are introduced.

The partition function  $\mathcal{Z}$  describing the conformational entropy of the polymer can be built up from the individual forward and backward partition functions. Given a chain starting point  $\mathbf{r}_0$ , the partition function describing the number of chain arrangements or paths of length  $s$  monomer units that start at  $\mathbf{r}_0$  and end at some position  $\mathbf{r}$  is denoted  $Q(\mathbf{r}_0, \mathbf{r}, s)$  (see figure 2.6). This function is weighted by the mean field according to how ‘acceptable’ each path is.  $Q(\mathbf{r}_0, \mathbf{r}, s)$  satisfies a modified diffusion equation (see Doi and Edwards [6] for derivation):

$$\frac{\partial Q(\mathbf{r}_0, \mathbf{r}, s)}{\partial s} = \frac{b^2}{6} \nabla^2 Q(\mathbf{r}_0, \mathbf{r}, s) - w(\mathbf{r}, s)Q(\mathbf{r}_0, \mathbf{r}, s)$$

With an initial condition  $Q(\mathbf{r}_0, \mathbf{r}, 0) = \delta(\mathbf{r} - \mathbf{r}_0)$ .  $w(\mathbf{r}, s)$  is the mean potential acting on the particular monomer  $s$ , so if monomer  $s$  is an **A** monomer then  $w(\mathbf{r}, s) = w_A(\mathbf{r})$ .

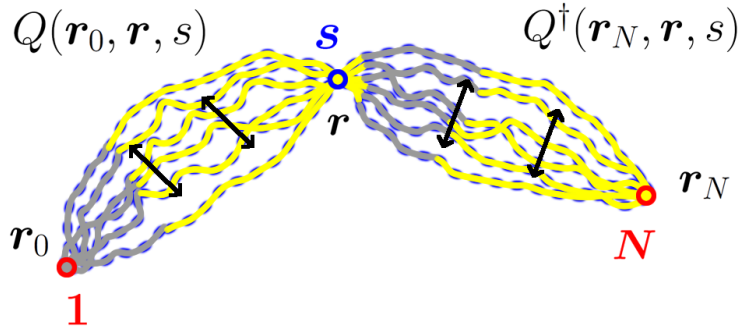


Figure 2.6: The forward partition function  $Q(\mathbf{r}_0, \mathbf{r}, s)$  effectively measures the number of possible chain arrangements with monomer  $s$  at position  $\mathbf{r}$  and the first monomer at position  $\mathbf{r}_0$  (first half of polymer chain in diagram). There is similarly a backward partition function  $Q^\dagger(\mathbf{r}_N, \mathbf{r}, s)$  measuring the possible chain arrangements beginning at the end of the chain. These functions are also weighted according to the mean field and polymer density field.

For a completely free polymer, the chain is allowed to begin at any point in space, and hence the function of interest is the partition function integrated over all starting positions, or the *forward propagator* (figure 2.7):

$$q(\mathbf{r}, s) = \int_V Q(\mathbf{r}_0, \mathbf{r}, s) d\mathbf{r}_0$$

This function now describes the number of paths starting at any point that reach some position  $\mathbf{r}$  in  $s$  monomer steps, weighted by the mean field. Clearly, this function satisfies the same modified diffusion equation:

$$\frac{\partial q(\mathbf{r}, s)}{\partial s} = \frac{b^2}{6} \nabla^2 q(\mathbf{r}, s) - w(\mathbf{r}, s) q(\mathbf{r}, s) \quad (2.9)$$

with initial condition  $q(\mathbf{r}, 0) = 1$ .

There is a corresponding *backward propagator*  $q^\dagger(\mathbf{r}, s)$ , being the integrated partition function beginning at the end of the chain (again at any point) and reaching any point  $\mathbf{r}$  in  $N - s$  monomer steps. This satisfies a similar diffusion equation with the initial condition  $q^\dagger(\mathbf{r}, N) = 1$ , where  $N$  is the final monomer of the chain.

The forward and backward propagator functions can be simply multiplied together and integrated over all space to obtain the total partition function  $\mathcal{Z}$ . In simpler terms, the total number of conformations or paths available to the polymer, is the number of paths from the beginning of the chain ( $q$ ) multiplied by the

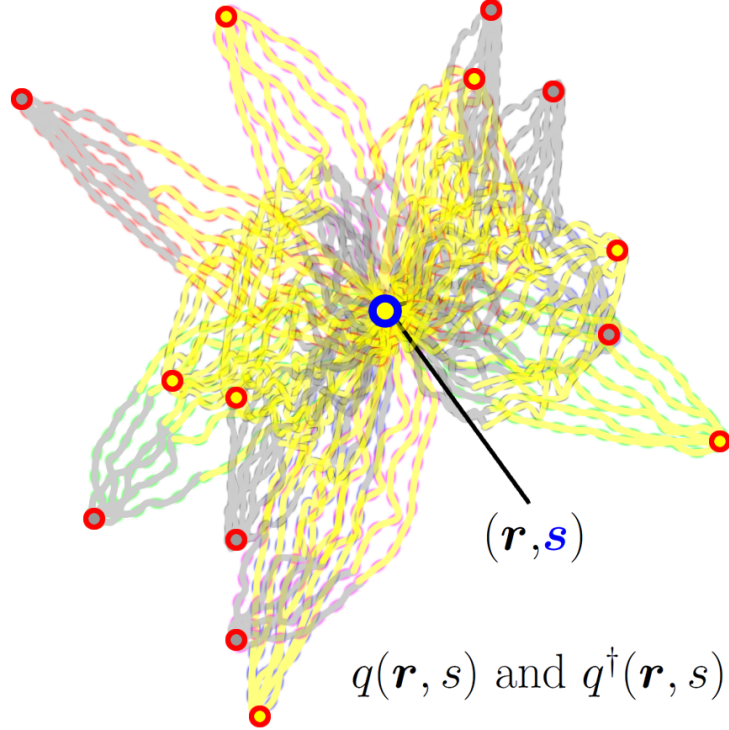


Figure 2.7: The polymer chain is free and is allowed to begin and end anywhere, so the forward and backward partition functions are integrated over start and end positions to give the *forward and backward propagators*  $q(\mathbf{r}, s)$  and  $q^\dagger(\mathbf{r}, s)$ . These functions describe the total number of polymer arrangements that place monomer  $s$  at position  $\mathbf{r}$ .

number of paths from the end of the chain ( $q^\dagger$ ):

$$\mathcal{Z} = \int_V q(\mathbf{r}, s) q^\dagger(\mathbf{r}, s) d\mathbf{r}$$

This integral is independent of the monomer step  $s$  considered. If the final monomer  $N$  is chosen, then due to the initial condition  $q^\dagger(\mathbf{r}, N) = 1$ :

$$\mathcal{Z} = \int_V q(\mathbf{r}, N) d\mathbf{r}$$

### 2.2.5 Connecting the propagator and the polymer density

If the forward and backward propagators are known, a corresponding polymer density can be obtained. The number of polymer chain states that have a particular

monomer  $s$  at any position  $\mathbf{r}$  is given by  $q(\mathbf{r}, s)q^\dagger(\mathbf{r}, s)$ . Dividing by the total partition function gives the probability of the  $s$ th monomer being at any point  $\mathbf{r}$ :

$$p(\mathbf{r}, s) = \frac{q(\mathbf{r}, s)q^\dagger(\mathbf{r}, s)}{\int q(\mathbf{r}, N)d\mathbf{r}}$$

Hence the density field of that particular monomer can be obtained by multiplying by the volume of the monomer  $v$ :

$$\phi(\mathbf{r}, s) = v \frac{q(\mathbf{r}, s)q^\dagger(\mathbf{r}, s)}{\int q(\mathbf{r}, N)d\mathbf{r}}$$

Adding all these monomer density contributions together gives the density fields  $\phi_A$  and  $\phi_B$ .

These formulas for the propagators and density fields form the theoretical and mathematical basis for the self consistent field theory computer simulation method. Chapter 4 describes the implementation of this mathematical basis into the simulation method.

# Chapter 3

## Theoretical Free Energy Models

The preliminary results section below shows self consistent field theory (SCFT) simulation images of several conformations formed by asymmetric block copolymers in poor solvents. In general, the species with shorter blocks (species **A**) forms a number of domains on the surface of a globule of the species with longer blocks (species **B**). This chapter develops a theoretical free energy model that describes this general conformation. The model is termed the *lens model*, since the surface **A** domains are similar to lenses. The lens model provides a theoretical prediction of the number of **A** domains or lenses formed on the surface of the larger **B** sphere.

A second free energy model is developed describing the *reverse conformation* of a small central **A** globule surrounded by the larger **B** species. A comparison between this *micelle model* and the lens model explains why the smaller **A** species always appears on the surface of the **B** globule and not in the center.

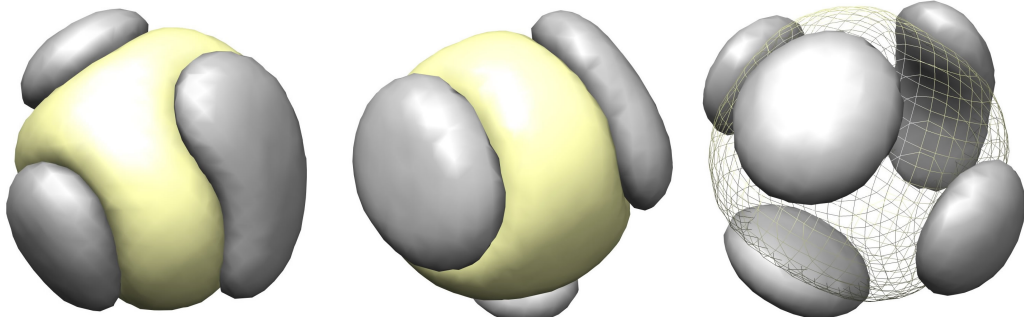


Figure 3.1: SCFT simulation images for polymer configurations: **Left:**  $N = 6000$ ,  $n = 16$ ,  $\mathcal{R} = 0.55$ ,  $\chi = 0.65$ ,  $\chi_{AB} = 0.25$ . **Middle:**  $N = 7000$ ,  $n = 14$ ,  $\mathcal{R} = 0.45$ ,  $\chi = 0.65$ ,  $\chi_{AB} = 0.3$ . **Right:**  $N = 8192$ ,  $n = 16$ ,  $\mathcal{R} = 0.45$ ,  $\chi = 0.65$ ,  $\chi_{AB} = 0.25$ .

### 3.1 Preliminary Results

Figures 3.1 and 3.2 show SCFT simulation images (see chapter 4) of collapsed asymmetric block copolymers in poor solvents. In all cases the smaller grey species **A** forms domains on the surface of the larger yellow species **B**. The polymer configurational parameters for each conformation are shown in the figure caption. For highly asymmetric block copolymers where the block size ratio is small, the total volume of the **A** species is small and the number of surface domains is in general large. A simple theoretical free energy model is developed to explain the formation of these conformations and their dependence on the polymer parameters.

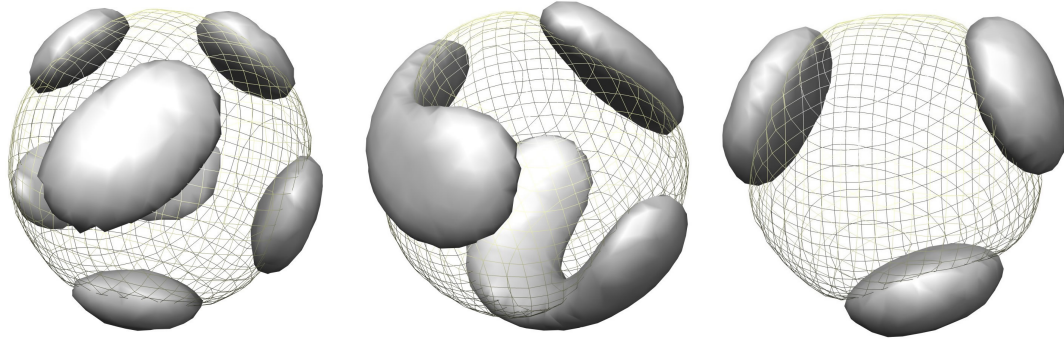


Figure 3.2: SCFT simulation images for polymer configurations: **Left:**  $N = 9284$ ,  $n = 22$ ,  $\mathcal{R} = 0.25$ ,  $\chi = 0.7$ ,  $\chi_{AB} = 0.2$ . **Middle:**  $N = 9000$ ,  $n = 18$ ,  $\mathcal{R} = 0.35$ ,  $\chi = 0.65$ ,  $\chi_{AB} = 0.2$ . **Right:**  $N = 5520$ ,  $n = 12$ ,  $\mathcal{R} = 0.3$ ,  $\chi = 0.7$ ,  $\chi_{AB} = 0.3$ .

### 3.2 Lens Model

A full theoretical description of the polymer systems is impossible. This thesis develops a simplified model of the polymer system that predicts the general characteristics.

The lens model consists of a sphere of species **B** in the middle with  $k$  *lens shaped* species **A** domains on the sphere surface (figure 3.3). The density of the sphere is taken as constant with the volume fraction of polymer  $\phi$  given in section 2.2.1.

The bulk shape of the polymer is modeled as a sphere of constant size and hence the free energy contribution due to the polymer-solvent surface interaction at the surface of the sphere is a constant with respect to the number of lenses  $k$ . For the purpose of predicting the number of lenses, the polymer-solvent interaction term in the free energy can be ignored. The important factor in determining how

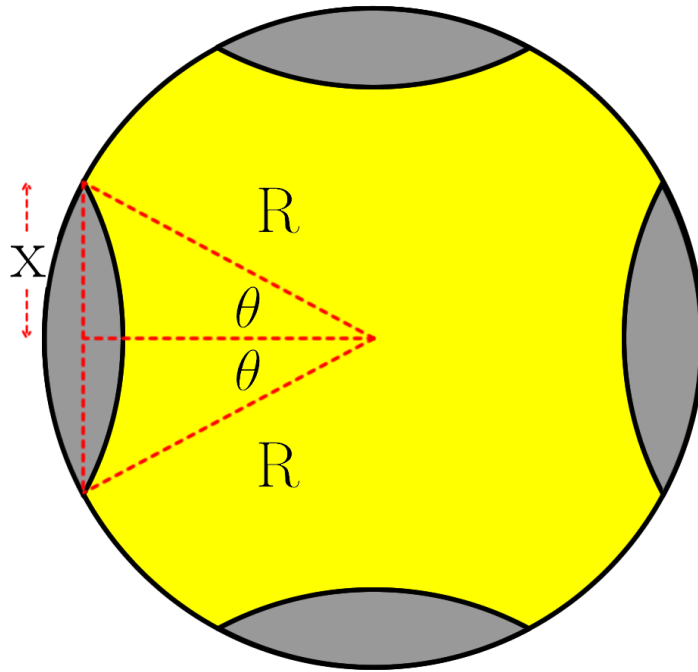


Figure 3.3: Lens model of the collapsed polymer. The yellow region is that of polymer species **B** and the grey species **A** forms  $k$  lenses on the surface

spherical the bulk polymer shape will be is the relative strengths of the **A-B** interaction ( $\chi_{AB}$ ) and the polymer-solvent interaction ( $\chi$ ). A high  $\chi$  indicates a large repulsive force between the solvent and polymer, and hence the free energy will be minimized by a conformation with minimum polymer-solvent contact, a sphere. However, the interaction between **A** and **B** blocks forces the blocks apart, creating elongated and distorted bulk shapes. In general, the polymer-solvent interaction is significantly stronger than the **A-B** interaction so the bulk shape is close to that of a sphere. This is confirmed in the majority of the simulation results (section 5.3.1), and consequently the spherical approximation is justified.

The **A** lenses are assumed to be equal sized with the **A** monomers and blocks equally distributed among them. This is a significant simplification of the system, as for some cases it could be impossible to equally distribute the **A** blocks among the lenses. This block distribution problem has been seen in the simulations, where some conformations result from impossible distributions of blocks between the **A** domains. (see section 5.5)

The two contributions to the free energy of the lens model are the surface tension between species **A** and species **B** on the inner surfaces of the lenses, and the chain stretching of the blocks in each species. The following sections give

the formulas for these free energy contributions and explain the results. A full derivation of the equations is given in appendix 2. Units of  $k_B T$  are adopted throughout.

### 3.2.1 Surface tension

The surface tension free energy is the simplest term to evaluate as it only depends on the **A-B** interaction surface area and not specifically on the complex geometry of the chains themselves. The expression for the free energy loss resulting from an interface between two incompatible polymers was derived in 1971 by Helfand and Tagami [13]:

$$F_{\text{surf}} = \sqrt{\frac{\chi_{AB}}{6}} b \rho_0$$

This gives  $F_{\text{surf}}$  per unit area, where  $\rho_0$  is the number density of monomers and  $b$  is the monomer size. The bulk polymer sphere is of constant volume fraction  $\phi$ , so for any volume  $V$  within the sphere;  $\phi V = \frac{4}{3}\pi b^3 N$ , where  $N$  is the number of monomers in the volume. As  $\rho_0 = \frac{N}{V} = \frac{3\phi}{4\pi b^3}$ , the total surface tension free energy for an **A-B** interaction surface area  $A$  is:

$$F_{AB} = \frac{3}{4\pi\sqrt{6}} \chi_{AB}^{1/2} \phi \frac{A}{b^2} \quad (3.1)$$

For the lens model with  $k$  lenses of radius  $x$  where the radius of the bulk sphere is  $R$ , the total free energy resulting from **A-B** surface tension is given by (see appendix 2):

$$F_{AB} = \frac{3}{2\sqrt{6}} \chi_{AB}^{1/2} k \phi \left( 1 - \sqrt{1 - \frac{x^2}{R^2}} \right) \frac{R^2}{b^2} \quad (3.2)$$

### 3.2.2 Chain stretching

The stretching and structure of the polymer chain inside a globule is in general very complicated [16, 2]. Due to the poor solvent, the density of chain sections is quite high and tangles can form, resulting in different sections of the chain stretching in different ways. For the model, a simplified view is taken where each block inside the polymer globule is treated as stretching in its own section of volume in a linear manner. The ideal chain stretching equation 2.2 can be used. This simplification of the stretching energy is expected to predict the general trend in the change of the free energy with respect to the various parameters. The overall *magnitude* of the stretching free energy term may not be well predicted by this model. This magnitude can be corrected by using a fitting parameter determined by comparing the model to the simulations.

### Species B stretching

To model the stretching of species **B**, each *half B block* is treated as stretching away from its junction point with the neighboring **A** block on the surface of the lens. The half **B** block is grafted to the lens surface and stretches into an expanding cone shaped volume (figure 3.4).

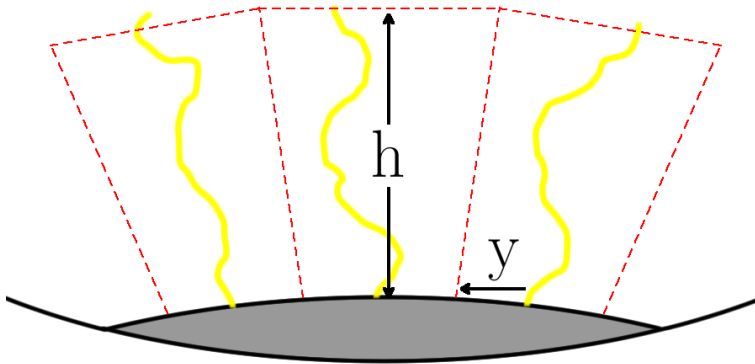


Figure 3.4: Species **B** stretching model. Each half **B** block is modeled as stretching into an expanding cone (red-dotted regions)

This is a simplified model of the physical stretching for several reasons. Firstly, it is geometrically impossible to fit the cone shaped volumes into the globule without overlap or left-over volume. This is ignored by setting the total cone volumes such that the overall volume of the **B** polymer is conserved. As the cone expands away from the lens, the main contribution to the stretching energy is from the portion of the half block closest to the lens surface. What happens at the large end of the cone, where these overlapping geometry effects originate, is less important.

Secondly, the outer ends of the half **B** blocks are not connected to the other half of their block. Again, this does not make much difference as the majority of the stretching energy comes from the portions near the lenses.

Finally, the final **B** block of the polymer chain is treated exactly the same as the other **B** blocks. Since it is only connected to an **A** block at one end, the second half of the block does not have a junction point and should not be anchored to a lens. Providing the number of blocks is large, this inconsistency in the last block becomes insignificant relative to the overall stretching energy.

The free energy resulting from stretching an ideal chain into a cone-shaped volume can be evaluated by generalizing the linear chain stretching energy given in the theory section (eq. (2.2)). This is done in appendix 2. Using the resulting

equation to evaluate the total stretching in the **B** blocks gives (appendix 2):

$$F_{SB} = \frac{8b^4 N_B R^4}{9h\phi^2 y^4} (R^{-3} - (R + h)^{-3}) \quad (3.3)$$

where  $N_B$  is the total number of **B** monomers. The height of each cone  $h$  is given by:

$$h = R \left( \left( \frac{4b^3 N_B}{n\phi y^2 R} + 1 \right)^{1/3} - 1 \right) \quad (3.4)$$

where  $n$  is the total number of blocks. The base radius of each cone  $y$  is:

$$y = R \sqrt{\frac{2k}{n} \left( 1 - \sqrt{1 - \frac{x^2}{R^2}} \right)} \quad (3.5)$$

### Species A stretching

The stretching of each *half A block* within the lenses is modeled as linear stretching into cylinders of equal height  $H$  (figure 3.5). The height of the cylinders is set by volume conservation in species **A**, and hence the over and under estimation of the heights of the cylinders is expected to cancel out.

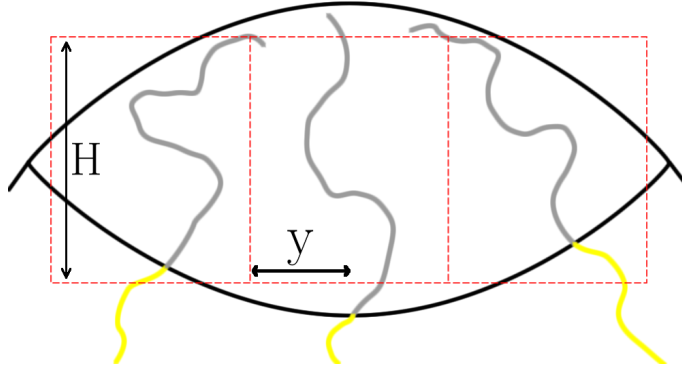


Figure 3.5: Species **A** stretching model. Each half **A** block is modeled as stretching in cylinders of equal height  $H$  (red-dotted regions)

Given that the **A** half blocks simply stretch in a linear manner, the ideal chain linear equation can be used directly (eq. (2.2)) giving a total stretching free energy in species **A** (see appendix 2):

$$F_{S\mathbf{A}} = \frac{8b^4 N_A}{3\phi^2 y^4} \quad (3.6)$$

Adding the surface tension (eq. (3.2)),  $\mathbf{B}$  stretching (eq. (3.3)) and  $\mathbf{A}$  stretching (eq. (3.6)) equations gives the total free energy of the lens conformation. The number of lenses  $k$  is a free variable, or correspondingly the lens size  $x$ .  $k$  is related to  $x$  via (appendix 2):

$$\frac{N_A}{kN} = 1 - \sqrt{1 - \frac{x^2}{R^2}} \left( 1 + \frac{x^2}{2R^2} \right) \quad (3.7)$$

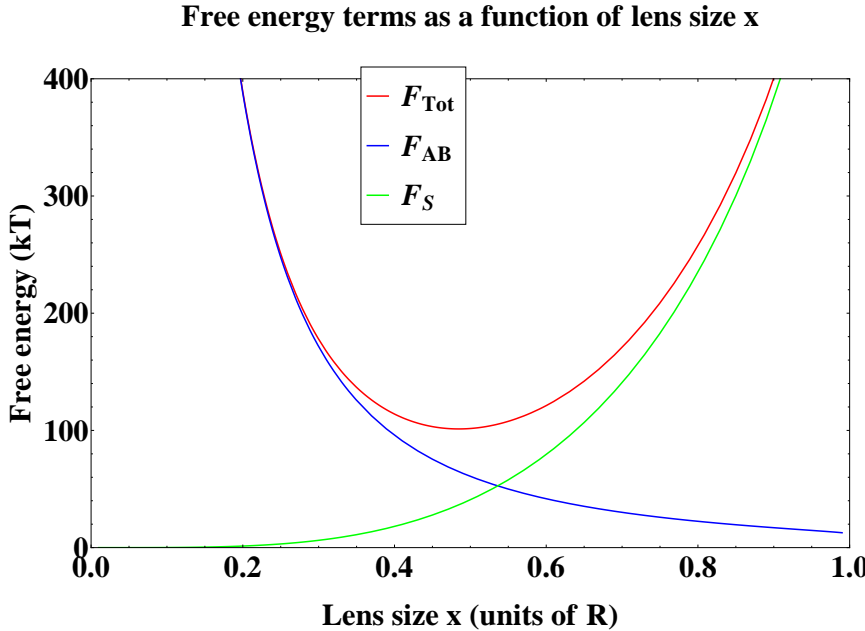


Figure 3.6: The surface tension, stretching and total free energy terms as a function of lens size  $x$  for a typical set of parameters.  $\mathcal{R} = 0.3$ ,  $\chi = 0.6$ ,  $\chi_{AB} = 0.2$ ,  $n = 20$ ,  $N = 5000$  and fitting parameter  $C = 2.2$

### 3.2.3 Summary

The total lens free energy is minimized with respect to the lens size  $x$ . Figure 3.6 shows typical plots of the surface tension ( $F_{AB}$ ), stretching ( $F_{S\mathbf{A}} + F_{S\mathbf{B}}$ ) and

total free energy terms as a function of lens size  $x$ . The minimum occurs as a result of the opposite trends of the surface tension and stretching terms. The five parameters  $N$ ,  $n$ ,  $\mathcal{R}$ ,  $\chi$  and  $\chi_{AB}$  are enough to completely define the polymer chain configuration, since the block size ratio  $\mathcal{R}$  and  $N$  determine  $N_A$  and  $N_B$ .

Only an integer number of lenses is possible. Consequently, there is a discrete set of possible lens sizes  $x$ . The free energy of each of these  $x$  values is calculated, giving a corresponding minimum free energy lens number  $k$  by equation (3.7). The lens model therefore gives a simple prediction of the *number of A domains* formed for a particular *asymmetric block copolymer chain*.

As discussed in section 3.2.2, it is difficult to estimate the overall magnitude of the stretching terms. A fitting parameter  $C$  is introduced to control this magnitude. In section 5.4, the fitting parameter is determined by comparing the predictions of the model to the results of the simulations.

The following phase diagrams show the trends predicted by the model.

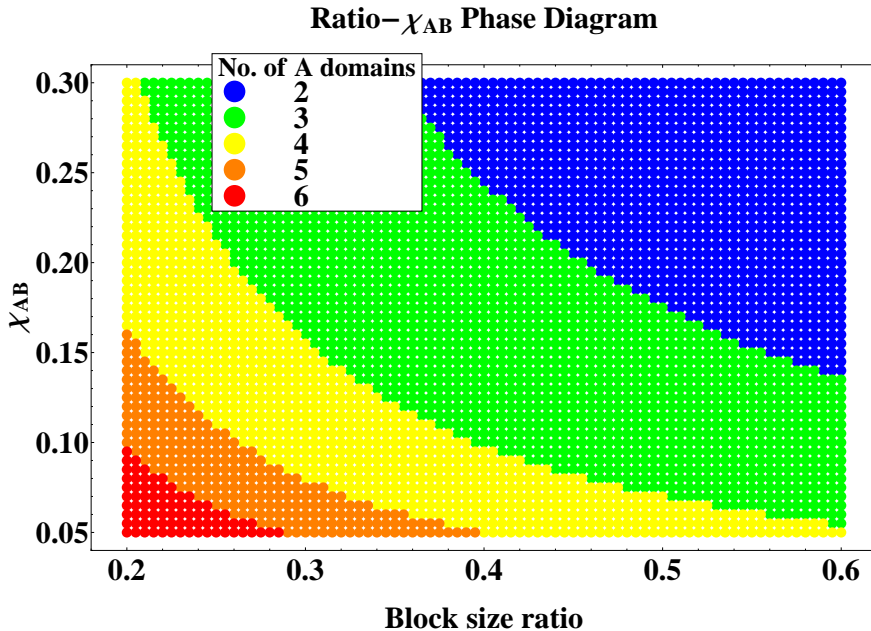


Figure 3.7: A phase diagram showing the number of **A** domains as a function of block size ratio and  $\chi_{AB}$ .  $N = 5520$ ,  $n = 12$ ,  $\chi = 0.7$ ,  $C = 2.2$ .

Figure 3.7 shows the trend of number of **A** domains with respect to  $\chi_{AB}$  and the block size ratio  $\mathcal{R}$ . As  $\mathcal{R}$  decreases, the number of **A** domains increases. For small block ratios, where the **A** blocks are quite short, a significant stretching free energy penalty results if the **A** blocks combine into less lenses. The stretching terms

overpower the surface tension term keeping the **A** species together to minimize **A-B** surface area. The result is an increase in the number of **A** domains.

The phase diagram also shows that as  $\chi_{AB}$  increases, the number of **A** domains decreases. This is due to the increase in repulsion between the **A** and **B** species and the increase in the surface tension free energy. The surface tension term overpowers the stretching terms and the number of **A** lenses decreases to minimize **A-B** surface area.

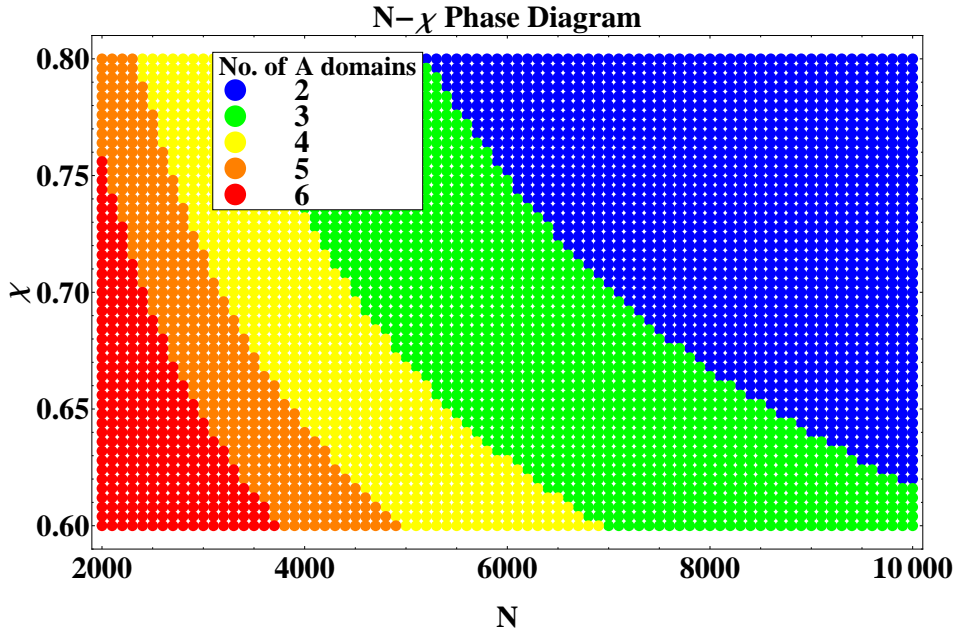


Figure 3.8: A phase diagram showing the number of **A** domains as a function of total monomer number  $N$  and  $\chi$ .  $\mathcal{R} = 0.4$ ,  $n = 12$ ,  $\chi_{AB} = 0.15$ ,  $C = 2.2$ .

Figure 3.8 shows the trend for number of **A** domains with respect to  $N$  and  $\chi$ . In order to gain an understanding of the trend, it is necessary to examine the free energy equations given above. Eliminating constants and parameters that don't depend on  $\chi$  and  $N$ , and noting that approximately:

$$y \propto R, h \propto R, N_A \propto N, N_B \propto N \text{ and } R \propto \left(\frac{N}{\phi}\right)^{1/3}$$

The stretching and surface tension contributions to the free energy become (equa-

tions (3.2), (3.3) and (3.6)):

$$F_{AB} \propto k\phi \left( 1 - \sqrt{1 - \frac{x^2}{R^2}} \right) R^2 \approx \phi R^2 \propto N^{2/3} \phi^{1/3}$$

$$F_{S\mathbf{A}} + F_{S\mathbf{B}} \propto \frac{N}{\phi^2 R^4} + \frac{N}{R\phi^2} (R^{-3} - (R+h)^{-3}) \approx \frac{2N}{\phi^2 R^4} \propto \frac{1}{N^{1/3} \phi^{2/3}}$$

From these relations, it can be seen that as  $N$  increases, the surface tension increases. This is due to the overall size of the polymer increasing, meaning the **A-B** interaction surface area also increases. The stretching energy correspondingly decreases, because there are more monomers in each block and hence it costs less energy to stretch them. The number of **A** domains then decreases with increasing  $N$ , as the surface tension term begins to dominate.

As  $\chi$  increases the polymer density  $\phi$  increases. The surface tension free energy also increases, because there is a higher density of monomers near the **A-B** interaction surface. The stretching energy decreases, because there are more monomers in each block and it costs less energy to stretch them. So the number of **A** domains decreases with increasing  $\chi$ , as the surface tension dominates.

The final parameter  $n$  is a discrete parameter, as there must always be an integer number of blocks. As the block number increases the number of **A** domains increases. Each individual block has less monomers and hence the stretching energy increases, favoring more **A** domains. The block number also imposes a maximum on the number of **A** domains formed, that of the number of **A** blocks ( $\frac{n}{2}$ ).

These general polymer conformation trends predicted by the model are replicated by the simulation results (see chapter 5).

### 3.3 Micelle Model

The conformation modeled by the lens model, of a number of **A** domains on the surface of a **B** sphere, is seen in the vast majority of simulations where the polymer is highly asymmetric (see chapter 5). To explain this general conformation characteristic, a second very different model referred to as the *micelle model* is developed.

The lens type conformation modeled above differs from the conformation seen in the case of a similarly asymmetric *di-block copolymer melt*. In the high density melt, the copolymers can assemble into *micelle* structures where the smaller species forms a sphere in the center of the micelle. This is the inverse of the lens conformation, as the smaller **A** species is in the center of the globule. [32, 20, 22] (figure 3.9)

This difference in conformation between the melt and the single-chain case is due to the following factors:

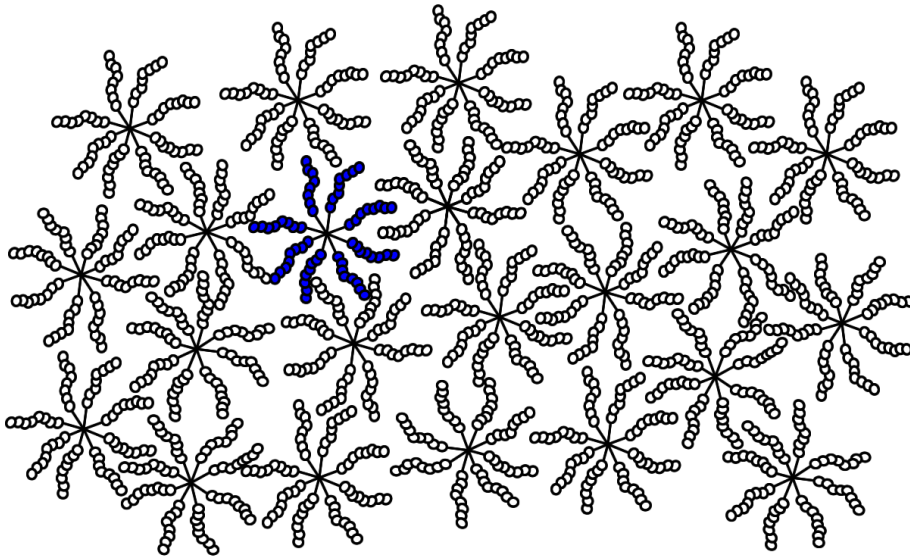


Figure 3.9: A micelle structure formed inside a *di-block copolymer melt*. The **A** blocks (solid lines) are shorter than the **B** blocks (balls), as in the case of the single asymmetric block copolymer chains modeled in this thesis.

- Polymer connectivity: the melt consists of many different polymer chains not connected, hence there are many free ends that don't exist in the single copolymer case.
- Poor solvent effect: in the polymer melt system, there is no explicit solvent. Each polymer chain exists in an environment surrounded by identical neighbors, and hence there is no tendency to collapse or become crushed. The outer ends of the copolymers can expand into the surrounding space without free energy penalty. The tendency of single chains in poor solvents to collapse is the main reason why the single copolymer chain behaves differently to the melt.

The free energy of the corresponding micelle structure for a single copolymer chain in a poor solvent is calculated and compared to the lens model. In this micelle model, the bulk structure of the polymer is again modeled as a sphere of constant volume fraction  $\phi$ . However, now the smaller species **A** forms a sphere *in the center* of the larger species **B**. This comparison provides an insight into why the smaller species in single chain asymmetric copolymers always appears on the surface of the globule.

As the bulk structure is still a sphere in the micelle model, the polymer-solvent surface tension interaction is a constant and comparisons between this system and the lens system can be made easily. Detailed calculations for the micelle model can be found in appendix 2.

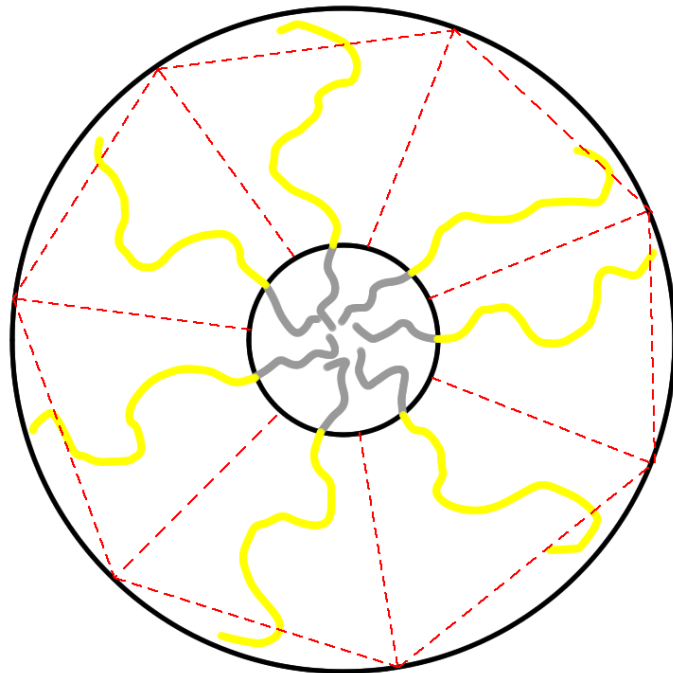


Figure 3.10: The micelle model. The smaller species **A** simply forms a sphere in the center of the larger **B** sphere. The **A** stretching is similar to the **A** stretching in the melt case as the chain ends lie close to each other (almost connected) in the center of the sphere. Each **B** half block is modeled as stretching away from species **A** in a cone (red-dotted regions).

### 3.3.1 Surface tension

The **A-B** surface tension free energy is given by (appendix 2):

$$F_{AB} = \frac{3}{\sqrt{6}} \chi_{AB}^{1/2} \phi^{1/3} N_A^{2/3} \quad (3.8)$$

### 3.3.2 Species A stretching

The central species **A** stretching free energy is modeled as being similar to stretching in the *melt micelle* case. The species **A** polymer segments stretch inwards from their junction points on the surface of the sphere so that their ends lie in the vicinity of the sphere center. The ends are therefore close to being connected, as they should be in the single chain case. (figure 3.10) The small species stretching inside a micelle has been calculated by Semenov [32] and is given by:

$$F_{S\mathbf{A}} = \frac{3\pi^2}{80} Q \frac{R_A^2}{N_{MA} b^2}$$

Where  $Q$  is the number of independent chains in the micelle. This is equivalent to the number of species **A** half blocks (of length  $N_{MA}$ ) in the single chain case. Hence the **A** stretching energy is:

$$F_{S\mathbf{A}} = \frac{3\pi^2}{80} \frac{n}{(N_A/n)b^2} \frac{b^2 N_A^{2/3}}{\phi^{2/3}} = \frac{3\pi^2 n^2}{80 N_A^{1/3} \phi^{2/3}} \quad (3.9)$$

### 3.3.3 Species B stretching

Stretching in species **B** is treated similarly to the lens case, with half blocks stretching away from their junction points on the surface of the **A** sphere into expanding cones. This gives (appendix 2):

$$F_{S\mathbf{B}} = \frac{2b^4 n N_B}{9\phi^2 h R_A^3} \left( 1 - \left( 1 + \frac{h}{R_A} \right)^{-3} \right) \quad (3.10)$$

where

$$h = R_A \left( \left( \frac{b^3 N_B}{R_A^3} + 1 \right)^{1/3} - 1 \right)$$

Adding equations (3.8), (3.9) and (3.10) gives the total free energy for the micelle model. The same fitting parameter  $C$  as that used in the lens model is used to control the magnitude of the stretching free energy terms.

## 3.4 Micelle-Lens Comparison

The free energies obtained for the micelle model and the lens model were compared for the entire parameter range considered in this thesis using a computer. It was

found that the lens model had a lower free energy in nearly every case, explaining why the simulations always produce conformations similar to the lens model.

The only extreme case found where the micelle model has a lower free energy than the lens model is in the limit of high monomer number  $N$  ( $= 10000$ ), high  $\chi$  ( $= 0.8$ ), low ratio  $\mathcal{R}$  ( $= 0.2$ ), high block number  $n$  ( $= 24$ ) and high  $\chi_{AB}$  ( $= 0.3$ ). A plot of the different free energy terms of both the lens and micelle models as a function of block size ratio in this extreme parameter range is shown in figure 3.11.

### Micelle and Lens FE terms as a function of ratio

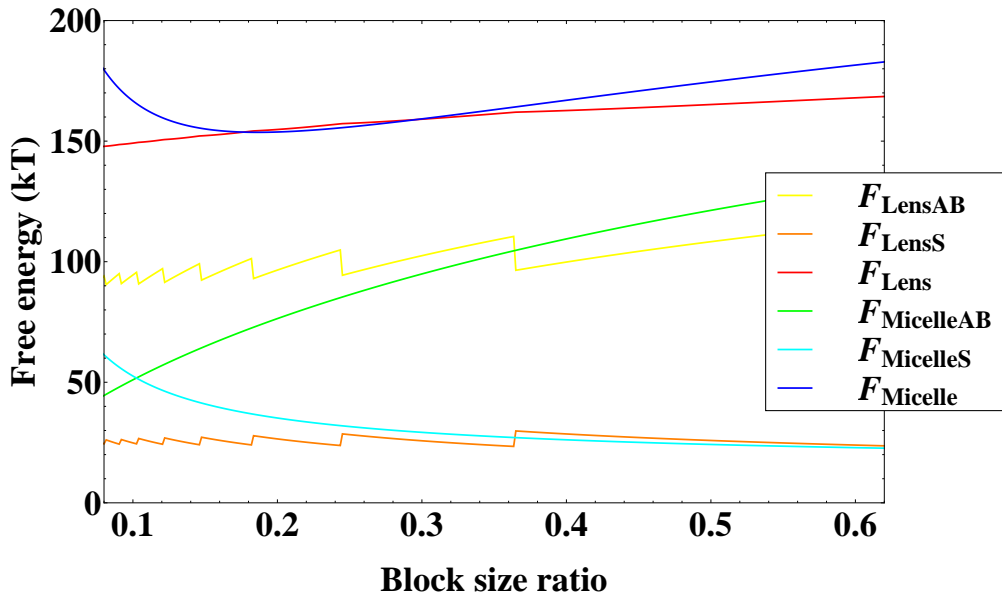


Figure 3.11: A plot of the stretching, surface tension, and total free energy terms for both the lens and micelle models as a function of block size ratio  $\mathcal{R}$ . The upper two lines are the total free energy for both models, the middle two lines are the surface tension free energy terms and the lower two lines are the stretching free energy terms.  $N = 10000$ ,  $n = 24$ ,  $\chi = 0.8$ ,  $\chi_{AB} = 0.3$  and  $C = 2.2$ . The sudden jumps in the lens model surface tension and stretching energy are a result of a jump from one integer number of lenses  $k$  to another. The region of interest is where the total micelle free energy drops below the total lens free energy, indicating it is the preferred conformation.

$N$ ,  $\chi$  and  $\chi_{AB}$  being large indicates that the polymer system is biasing towards

a large surface tension and a small stretching energy, as shown in the plot. In order for the micelle to have a lower free energy than the lens, the surface tension term must dominate.

However, for the **A-B** surface area of the sphere in the micelle to be less than the total **A-B** surface area of the lenses in the lens model, there must be many lenses. The block size ratio must be small and the number of blocks large. Clearly, if this goes too far, then the stretching energy of the micelle increases too much, as can be seen in the steep rise of  $F_{\text{Micelle}}$  for block size ratios less than 0.15.

It would be interesting to investigate this transition further and see if it is possible to get a conformation similar to the micelle in the case of single chain block copolymers in poor solvents. Unfortunately, it is very difficult to get the simulations to converge in this extreme region of the parameter space (see section 5.1). If the simulation method could be improved further, then an investigation of this transition could be possible.

The surface tension terms for the two models shown in figure 3.11 are directly proportional to the amount of **A-B** surface area. This emphasizes an important aspect of this comparison. In the case of a liquid system (non-connected monomers) of the same conformation as the micelle, the species **A** ball would never be located in the center of the **B** sphere. Instead it would sit against the inner surface of the sphere, effectively forming the lens model with  $k = 1$ . This would reduce the **A-B** surface area without any other losses of free energy. In general, the strength of the surface tension term is greater than that of the stretching terms. An example can be seen in figure 3.6, where at the minimum, the  $F_{AB}$  term is around twice the  $F_S$  term (despite the fitting parameter  $C$  doubling  $F_S$ ). This indicates that in general it is more important that the **A-B** area is minimized. It becomes clear that a conformation with the **A** species on the surface, which minimizes **A-B** contact effectively for ‘free’, has a lower free energy.

These simple free energy models explain why the **A** species is nearly always seen to form domains *on the surface* of the **B** sphere and not in the center. The presence of the **A** species on the surface of the sphere *minimizes the A-B surface tension interaction*.



# Chapter 4

## Self Consistent Field Theory Implementation and Method

This chapter gives a detailed description of the *self consistent field theory* (SCFT) simulation method. This simulation method predicts the conformations formed by single-chain asymmetric block copolymers in poor solvents. These predictions can be compared to the theoretical free energy model developed in the previous chapter and an understanding of the polymer system can be reached.

This chapter outlines the simulation process and gives the method used for solving the propagator equation. Code optimizations are also described. The simulation method is technically complex and only the main ideas are summarized here. More information on the use of SCFT for simulation of *polymer melts* can be found in references. [10, 19, 8, 28, 26]

As outlined in the theory section 2.2, SCFT is based on the density field representation of the polymer. The density fields  $\phi_A(\mathbf{r})$  and  $\phi_B(\mathbf{r})$  denote the densities of polymer species **A** and **B** at each lattice point, with the solvent density given by  $\phi_S = 1 - \phi_A - \phi_B$ . However, with the density field representation the notion of a *connected polymer* is lost. This polymer connectedness is returned with the statistical *forward and backward propagators*. This process is shown in figure 4.1.

The main technical steps in the method are:

1. Start with random initial density fields  $\phi_A$  and  $\phi_B$
2. Calculate the mean potentials  $w_A$  and  $w_B$  generated by these density fields (with equations (2.7) and (2.8))
3. Calculate the forward and backward propagators along the polymer chain given the mean potentials using the *propagator equation* (eq (2.9)). (This returns the connected polymeric nature to the density fields)

4. Find new density fields via:

$$\phi(\mathbf{r}, s) = v \frac{q(\mathbf{r}, s) q^\dagger(\mathbf{r}, s)}{\int q(\mathbf{r}, N) d\mathbf{r}}$$

5. Use these new density fields in the first step

After many iterations the density fields generally converge to a fixed point where the input density fields  $\phi_A$  and  $\phi_B$  of each iteration are very similar to the output fields. The mean potentials become self consistent, leading to the name of the simulation method.

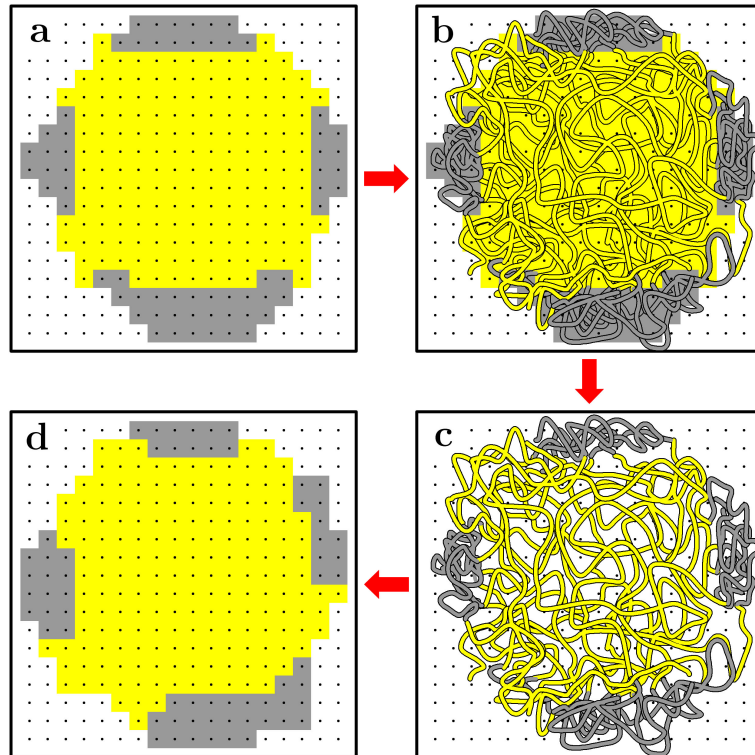


Figure 4.1: The SCFT Iterative process: Starting with a polymer density field (a), one iteration of SCFT propagates all possible chains through the density field (b) and gives each a weighting factor. A weighted average is then performed over all these possible chains (c) to give a new density field (d). The propagator steps (b) and (c) ensure that the density fields  $\phi_A$  and  $\phi_B$  describe a *connected polymer chain*.

## 4.1 Simulation Process

Figure 4.2 shows a detailed flow chart of the processes and steps involved in the method. There are two main loops, *the iterative loop* and the *step loop*. The iterative loop describes the iterative procedure of approaching equilibrium by generating full new density fields via the propagator and mean potentials. The step loop propagates the polymer through the mean potentials by solving the propagator equation at each step along the chain. The lattice box size used is  $51 \times 51 \times 51$  cubic units.

### 4.1.1 Initialization

The polymer densities  $\phi_A$  and  $\phi_B$  are initialized to random normalized fields within a sphere of radius  $\frac{2}{3}rds$  the half box side length (25), centered in the lattice box. The monomer size  $b$  is chosen such that the total polymer volume ( $vN$ ) is an 80th of the box volume, also setting the overall density normalization.

The forward and backward propagators  $q$  and  $q^\dagger$  are functions of position and monomer step along the chain. 500 total steps are used along the polymer chain, and hence each step does not necessarily correspond to one monomer. The number of monomers per step, or step size  $ds$ , is not constant along the chain. A smaller step size (i.e. more steps) is used inside the smaller **A** blocks as this is required to converge to a solution. (see section 5.1)

The propagators are initialized as 1 at every point, in accordance with the initial condition at each end of the chain in the propagator equation.

### 4.1.2 Iterative loop

Given input density fields  $\phi_A$  and  $\phi_B$ , one step of the iterative loop calculates the mean potentials, solves the propagator equation and produces new density fields. However, this is not split into distinct steps. If the entire propagator is solved from the beginning of the chain to the end, without updating the density and mean potentials along the way, then the density can grow too large at some points. The density information does not feedback to the propagator quickly enough. As a solution, the density contribution of each step is updated continually, as the propagator is solved along the chain. This stabilizes the process; the mean potentials now prevent large density accumulations from developing at any one point.

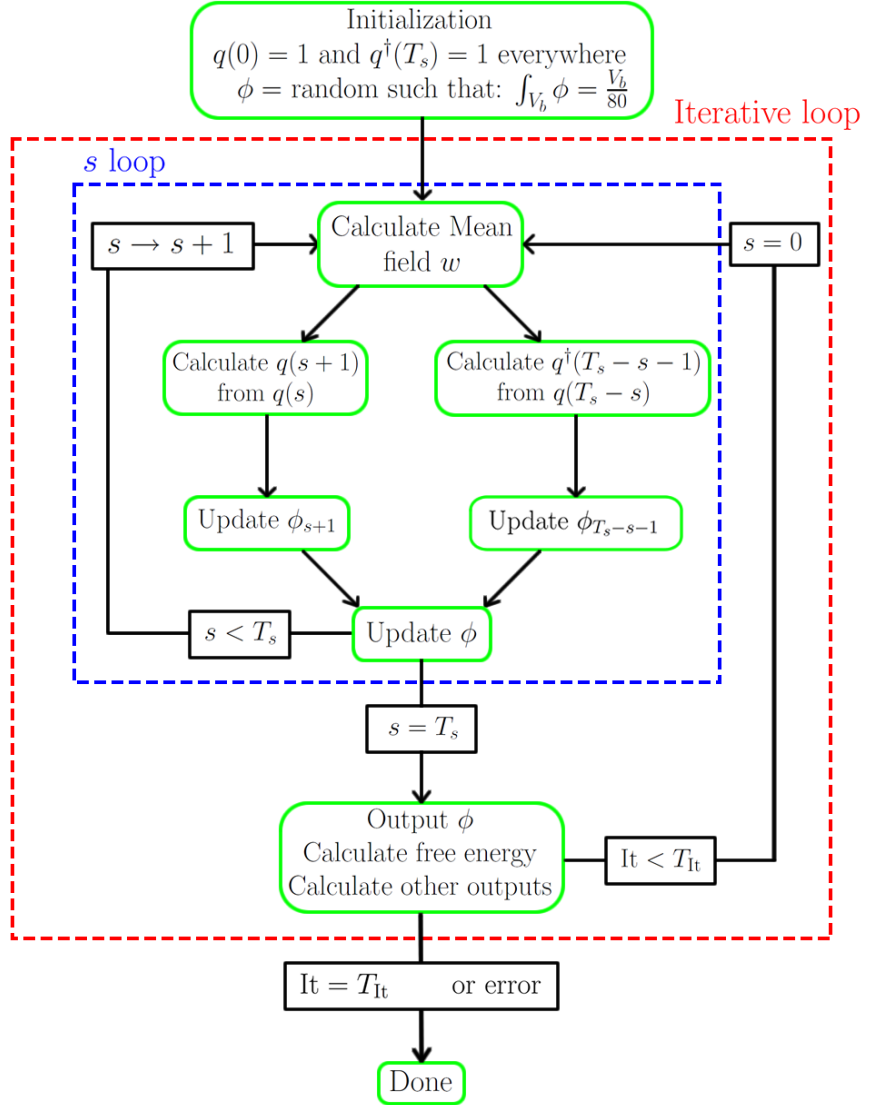


Figure 4.2: Flow diagram of simulation process showing the step loop and iterative loop.  $q$  and  $q^\dagger$  are the forward and backward propagators,  $s$  is the current step,  $It$  is the current iteration,  $\phi_s$  is the density contribution of the  $s$ th step,  $\phi$  is the total density ( $\phi_A$  and  $\phi_B$ ),  $T_s$  is the total steps and  $T_{It}$  is the total iterations.

### Step loop

As shown in the flow diagram 4.2, given a particular step  $s$ , the step loop solves for the forward propagator at step  $s + 1$  and simultaneously for the backward

propagator at step  $T_s - s - 1$ .  $T_s$  is the total number of steps, or the end step in the chain. Using these propagator values, the step density contributions  $\phi_{s+1}$  and  $\phi_{T_s-s-1}$  are updated using the equation:

$$\phi(\mathbf{r}, s) = v \frac{q(\mathbf{r}, s) q^\dagger(\mathbf{r}, s)}{\int q(\mathbf{r}, N) d\mathbf{r}}$$

This equation involves both the forward and backward propagators at step  $s$ . However, only  $q$  or  $q^\dagger$ , not both, are known at the current step. Hence the value from the *previous iteration* is used for the unknown function  $q$  or  $q^\dagger$ . This is an inevitable result of updating the density every step, but is actually advantageous, since it helps to stabilize the simulations.

Once the step densities  $\phi_{s+1}$  and  $\phi_{T_s-s-1}$  are updated, their contribution to the total densities  $\phi_A$  and  $\phi_B$  are updated. The mean potentials  $w_A$  and  $w_B$  are then recalculated from the new density fields, and used as the input fields for the next step.

## Data Output

Once the step loop for each iteration is completed, the final output density fields  $\phi_A$  and  $\phi_B$  are recorded in a form that can be displayed using the molecular visualization program **UCSF Chimera** [21]. The average and standard deviation of each density field is calculated to give information about how close to convergence the density fields are. The free energy of the conformation is also calculated (see section 4.3).

The amount of mixing between the two species is found to test the phase separation of the polymer species. This is calculated through the mixing parameter:

$$M = 4 \frac{\int \phi_A \phi_B d\mathbf{r}}{\int (\phi_A + \phi_B)^2 d\mathbf{r}}$$

(see Pinson & Williams [27] for an investigation of phase separation behavior in SCFT) This mixing parameter is used to differentiate between phase separated and homogenous density fields. If  $M$  is small (less than about 0.3), then the polymer species has not phase-separated and more iterations are required.

The simulation is run for up to 40 iterations to converge to a self consistent solution. The production runs discussed in the results chapter run for 25 iterations. The typical time length required at full resolution ( $51^3$  lattice points and 500 steps) for a run of 25 iterations is several hours, when run on a Linux computer cluster at the Australian National University [31]. The main time consuming task is calculating the solution to the propagator equation.

## 4.2 Solving the Propagator Equation

The main task of the self consistent field theory simulations is to solve the propagator equation:

$$\frac{\partial q(\mathbf{r}, s)}{\partial s} = \frac{b^2}{6} \nabla^2 q(\mathbf{r}, s) - w(\mathbf{r}, s)q(\mathbf{r}, s)$$

Where  $w(\mathbf{r}, s) = w_A$  if  $s$  is in an **A** block, and  $w_B$  if  $s$  is in a **B** block. The derivation of the solution to this equation is quite involved and is given in appendix 1. The solution is:

$$q(\mathbf{r}, s + \delta s) = \gamma \exp\left(\delta s \frac{b^2}{6} \nabla^2\right) q(\mathbf{r}, s)$$

where  $\gamma = \exp\left(-\delta s \exp\left(\frac{\delta s}{2} \frac{b^2}{6} \nabla^2\right) w(\mathbf{r})\right)$

The exponential is calculated through:

$$\exp\left(\delta s \frac{b^2}{6} \nabla^2\right) q(\mathbf{r}, s) = \left(\frac{3}{2\pi\delta s b^2}\right)^{3/2} \int \exp\left(-\frac{3|\mathbf{r} - \mathbf{r}'|^2}{2b^2\delta s}\right) q(\mathbf{r}', s) d\mathbf{r}' \quad (4.1)$$

And similarly for the exponential in the coefficient  $\gamma$  with  $\delta s \rightarrow \frac{\delta s}{2}$  and  $q(\mathbf{r}', s) \rightarrow w(\mathbf{r})$

The gaussian integral in (4.1) could be calculated by simply summing the relevant quantities over the entire lattice. However, this would be very time consuming as the entire lattice must be integrated ( $\mathbf{r}'$ ) for every single point in the lattice ( $\mathbf{r}$ ) ( $\propto 51^6$  calculations per step). Clearly, due to the exponential factor, only points inside a certain radius  $R_{max}$  have a significant contribution to the integral and need to be included.

In addition to this simplification, a *randomized integration method* is used to sum the points within  $R_{max}$  [27]. For each integer lattice radius from the middle point ( $\mathbf{r}$ ), several points are randomly chosen to represent the contribution of *all points* at this radius. Through appropriate normalization, these random points approximate the entire discrete integral (see figure 4.3). The accuracy of this approximation can be improved by increasing the number of random points taken at each radius. It was found that 2 random points per lattice radius  $1, 2 \dots R_{max}$  is sufficient. This method drastically increases the speed of the simulations as only 2 points are summed at each radius  $R$  instead of on the order of  $R^3$  points.

This integral is performed for every point  $\mathbf{r}$  within the box to give  $q(\mathbf{r}, s)$ . The propagator is taken as 0 for points *outside the box* that should contribute to the integral, since the polymer cannot be allowed outside the box. For the calculation of the coefficient  $\gamma$ , the mean potential outside the box is taken as  $\chi$ , as the polymer density is 0.

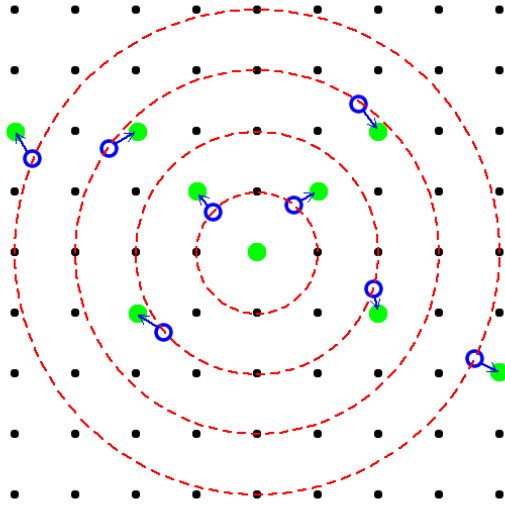


Figure 4.3: Calculation of the gaussian integral in equation (4.1) by a randomized integration method. At each lattice radius  $1, 2 \dots R_{\max}$  (red-dotted circles) two random points (blue circles) are chosen and rounded to the nearest lattice site (green points). The resulting sites are appropriately averaged to give the total integral.

After the calculation for each step, the forward and backward propagators are both normalized again to prevent large values developing. This does not effect the simulation as the total partition function  $\mathcal{Z}$  cancels the  $q$  normalization when the new density fields are calculated.

### 4.3 Free Energy Calculation

In some cases during SCFT simulations it is possible for the polymer density fields to become stuck in *semi-stable* configurations. [10] One solution to this problem is to run the simulations many times from different random initial conditions and average the results. [26] However, due to the long computation times, this is not always possible. It is advantageous to calculate the free energy of a particular output conformation. This allows the true equilibrium conformations to be identified, as they will have a lower free energy than the semi-stable conformations.

The free energy of a particular density field can be calculated using equation

2.6:

$$F = -\log \left( \int_V q(\mathbf{r}, N) d\mathbf{r} \right) + \int_V [\phi_S (\log(\phi_S) - 1) + \chi (\phi_A \phi_S + \phi_B \phi_S) + \chi_{AB} \phi_A \phi_B] d\mathbf{r}$$

The terms in the second integral can be calculated from the density fields  $\phi_A$  and  $\phi_B$ . In order to calculate the conformational entropy term accurately, the forward propagator is solved again for every step, without updating the density continually. The magnitude of the term is then extracted from the re-normalization factors applied to  $q$  after each step.

### 4.3.1 Simple simulation check

It is possible to check the simulation method and the free energy calculation by performing simulations on the simple known case of an *ideal chain homopolymer*. For an ideal chain there are no interactions and the mean potential  $w$  is set to zero. By reducing the size of the simulation box, or equivalently increasing the size of the polymer, the free energy of a *crushed ideal chain* can be measured. Equation (2.3) gives the theoretical free energy of an ideal chain crushed into a sphere of radius  $R_c$ :

$$F(R_c) \propto k_B T \frac{R_0^2}{R_c^2}$$

The measured free energy should hence be proportional to  $R_c^{-2}$ . This test was performed on a range of chains with different natural sizes  $R_0$ . The polymer was allowed to reach equilibrium and the free energy measured for a range of small, spherical lattice sizes.

The left plot of figure 4.4 shows the free energy as a function of crushing scale  $R_g$  for polymers with a range of natural sizes  $R_0 = \sqrt{Nb^2}$ . The data points are fit with a model  $F = aR_g^{-2}$ , where  $a(R_0)$  is some fitting coefficient. Clearly the fit is very good. The upper right plot shows the  $R^2$  fitting goodness as a function of the natural size. As the natural size increases, the fit becomes better indicating that more highly crushed ideal chains obey the predicted law more closely. This is expected for low crushing, as the polymer can fluctuate more and hence the free energy calculation is not as accurate. The lower right plot shows the *fitting coefficient*  $a$  of the model as a function of natural size. This fitting parameter is proportional to  $R_0^2$ , as expected from equation (2.3). These plots show that the free energy calculation included in the simulation is accurate for the ideal chain case, constituting a check of the simulation method and the free energy calculation.

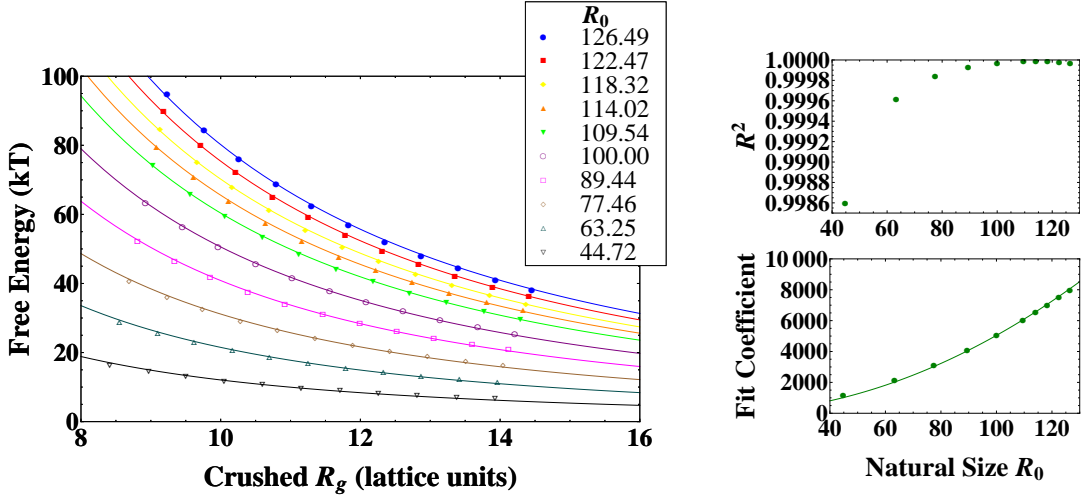


Figure 4.4: Crushing an ideal chain free energy test: the left plot shows the measured free energy as a function of crushed radius of gyration for a range of ideal chain natural sizes ( $R_0 = \sqrt{Nb^2}$ ). The data is fitted with model  $F = \frac{a}{R_g^2}$ . The  $R^2$  fitting goodness and the fitting coefficient  $a$  are plotted on the right for each natural size. The coefficient  $a$  is fitted with  $a = 0.504R_0^2$  ( $R^2 = 0.9998$ ).

## 4.4 Simulation Stability

The simulation method is inherently unstable and the density fields do not converge to equilibrium easily. There are problems with the density growing large at some points and causing the simulation to crash. The free energy calculation introduced above gives a measure of the simulation stability. As a function of iteration, the free energy should decrease as the density fields approach equilibrium and then reach a constant value at equilibrium. The following describe some of the methods and calculations developed to improve the stability of the simulations.

### 4.4.1 $\Delta\phi$ term

To increase the stability of the simulation, an artificial term is introduced to the mean potential that counteracts changes to the density. This term is proportional to the change in density from the previous step, and hence if the density changes suddenly between steps, the mean potential acts to reverse or prevent more change. The strength of the parameter is controlled by a  $\Delta\phi$  coefficient. Figure 4.5 shows the free energy as a function of iteration for a range of  $\Delta\phi$  coefficients, for a particular polymer configuration. Clearly when this coefficient is small or zero, the

simulation is unstable. As the coefficient increases the simulations become more stable and the free energy reaches an approximately constant value indicating the equilibrium configuration has been reached.

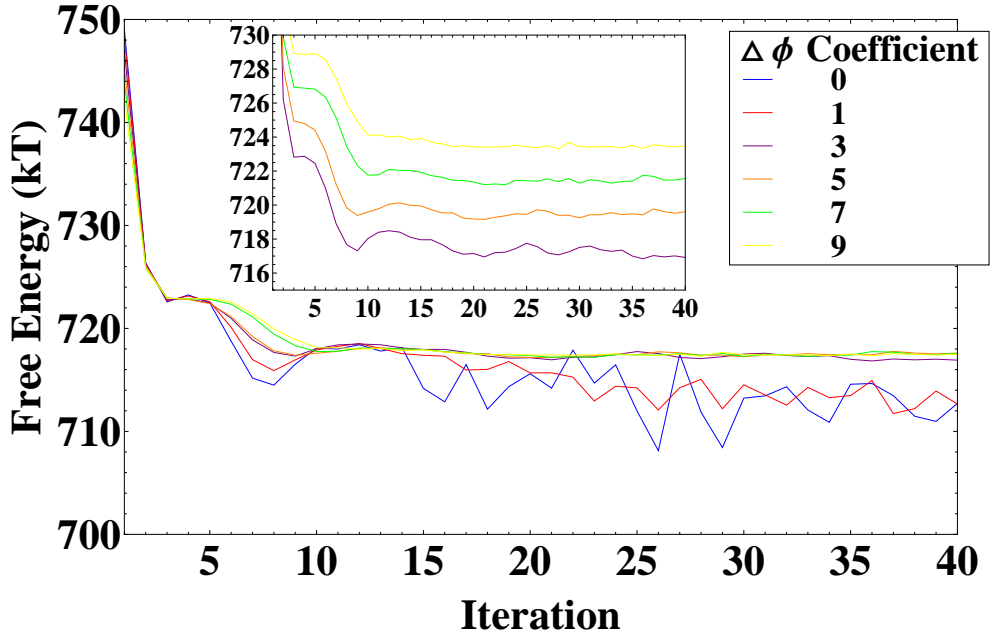


Figure 4.5: Example  $\Delta\phi$  coefficient test showing the free energy as a function of iteration number. The inset shows the higher coefficient graphs shifted apart vertically for ease of viewing. (Polymer:  $N = 1890$ ,  $n = 6$ ,  $\mathcal{R} = 0.4$ ,  $\chi = 0.7$ ,  $\chi_{AB} = 0.2$ )

This additional  $\Delta\phi$  term in the mean potential is not a physical term and can adversely affect the simulation. To be sure that the final equilibrium state is correct, the  $\Delta\phi$  term should become insignificant relative to the other mean potential terms. At equilibrium, the density is not changing, implying that the  $\Delta\phi$  term should be small. This was checked explicitly for a range of  $\Delta\phi$  coefficients by measuring the maximum ratio of the  $\Delta\phi$  mean potential term to the total mean potential.

The  $\Delta\phi$  coefficient for production runs is chosen to be 5, as this gives a stable free energy while having only a small effect on the final equilibrium state. For this coefficient, the maximum ratio of the  $\Delta\phi$  mean potential term to the total mean potential reduced to less than 0.6% at equilibrium for the configuration in figure 4.5.

In figure 4.5, the free energy of the unstable runs ( $\Delta\phi$  coefficient = 0 or 1) is

lower than the free energy of the stable runs. This indicates that these unstable runs are more correct, although clearly they are not at equilibrium. This problem could be due to rapid changes in the density fields causing an inaccurate free energy calculation. If there are large density gradients, then the calculation of the propagator is less accurate due to the finite step size. It is probable that the lower free energy of the unstable runs is an artifact of the finite step size in the propagator calculation.

#### 4.4.2 Other optimizations

##### Simple and Anderson mixing

Most SCFT simulations used in polymer physics do not continually update the density as the propagator is calculated. Instead, a method of *simple mixing* is used to stabilize the simulation. [8, 28] This involves calculating the mean potential from a combination of the new and old (previous iteration) density fields. The combination is heavily biased towards the old density fields and hence the mean potential changes only slightly after each iteration, stabilizing the simulation.

This was attempted in these simulations but it was found that the method discussed previously is more stable. It is possible that a more advanced version of simple mixing, such as Anderson mixing [35] could provide a more stable simulation.



# Chapter 5

## Results and Analysis

This chapter presents the results of the self consistent field theory simulations. These simulations provide a prediction of the conformations formed by asymmetric block copolymers in poor solvents. The results are analyzed and compared to the theoretical lens model. The results of the simulations and the model combine to provide a good understanding of the polymer system and allow accurate predictions of the conformations formed by physical asymmetric block copolymers in poor solvents.

### 5.1 Convergence Range

Five parameters completely determine the copolymer chain, monomer number  $N$ , polymer-solvent interaction strength  $\chi$ , polymer-polymer interaction strength  $\chi_{AB}$ , number of blocks  $n$  and block size ratio  $\mathcal{R} = \frac{N_A}{N_B}$ . Reaching a stable and valid polymer conformation using SCFT is only possible within certain ranges of these parameters. Outside of these ranges, either the polymer density gets large quickly and the simulation crashes, or the density does not collapse from an initial almost homogenous state in a reasonable number of iterations. These *non-convergence* and *fast-convergence* cases, and the parameter ranges in which they occur are detailed in this section. Similar problems have been studied elsewhere. [11]

The key quantities that determine whether the simulations converge are  $\chi N_A$  and  $\chi N_B$ . If there are relatively few monomers in a particular species, and  $\chi$  is small, then the ‘forces’ causing the polymer to collapse into a ball are small and the convergence happens slowly. Correspondingly, if there are many monomers and  $\chi$  is high, the convergence forces are large causing large density accumulations and crashing the simulation. These problems are exacerbated when the polymer configuration is highly asymmetric with a small  $\mathcal{R}$ . To make the shorter species **A** blocks converge,  $\chi$  must be high as  $N_A$  is small. However this makes  $\chi N_B$  large,

often crashing the simulations. Hence there is a lower limit on the block size ratio. Depending on the other parameters, it is difficult to simulate polymers with block size ratios below 0.3 or 0.4. For these small block size ratios, only a small range of  $\chi$  values can be used. In simulation runs,  $\chi$  values in the physically reasonable range of 0.6 to 0.85 were attempted. Typically for small  $\mathcal{R}$ , only one or two of these values were successful.

To counter this uneven convergence, a smaller step size is used for the **A** blocks while solving the propagator. The density is updated every step, so the **A** blocks are updated more often, causing them to converge faster than the **B** blocks. This method works quite well, although there is a limit to the difference in step sizes possible between the **A** and **B** blocks. Typically, for the small ratio values of 0.3 and 0.4, the step size in the **A** blocks is chosen as a little more than half that in the **B** blocks.

To produce an interesting conformation, the two polymer species must phase separate. If  $\chi_{AB}$  is too small, then the polymer acts as a homopolymer, forming a homogenous ball. If  $\chi_{AB}$  is too high, then the polymer species are forced apart violently, causing high density gradients between blocks and crashing the simulation. The  $\chi_{AB}$  range examined was  $0.1 < \chi_{AB} < 0.3$ .

Only conformations that appear stable over many iterations, and are sufficiently converged, are judged as valid. This can be a subjective process, but in general it is quite clear whether a particular result has converged. All borderline cases are rejected.

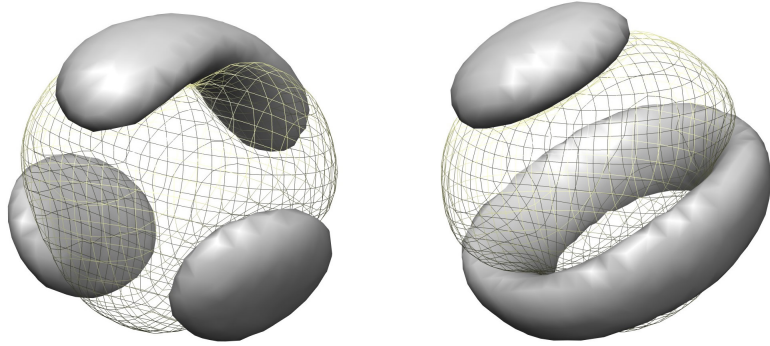


Figure 5.1: Two final conformations resulting from the same polymer configuration  $N = 7000$ ,  $n = 14$ ,  $\mathcal{R} = 0.5$ ,  $\chi = 0.65$ ,  $\chi_{AB} = 0.15$ . The free energies averaged over the last six stable iterations are:  $F_{\text{left}} = 3831.58 \pm 0.04$  and  $F_{\text{right}} = 3831.39 \pm 0.06$ . As the right conformation has a lower free energy, it is expected to be the true equilibrium conformation.

## 5.2 Reproducibility

In some cases, the conformations produced for the same polymer chain configuration by different simulation runs (different random initial density fields) differ. An example is shown in figure 5.1, with the free energies of the two conformations given in the figure caption. These conformations are similar in **A-B** surface area and total solvent-polymer surface area. The chain stretching energies for each conformation are likely to be similar. The free energy of the ring and ball conformation on the right has a slightly lower value, so the other conformation could be a non-equilibrium semi-stable configuration. Due to the similarity in the free energies, it is not surprising that both conformations are produced by the simulation. For cases such as this, the conformation with the lowest free energy is taken as correct. So for this polymer chain configuration, the value of 2 **A** domains is taken.

## 5.3 General Conformation Trends

### 5.3.1 Larger species centralized

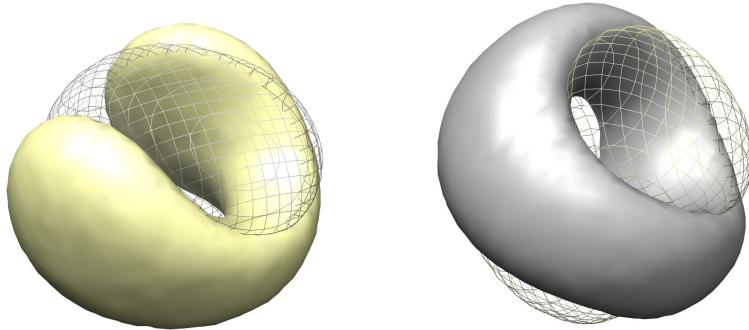


Figure 5.2: Conformations for high ratio polymer configurations: the left conformation is produced by a symmetric copolymer with **A** and **B** blocks of the same size ( $\mathcal{R} = 1$ ). The right is produced from a slightly asymmetric copolymer ( $\mathcal{R} = 0.95$ ). (Other parameters:  $N = 5520$ ,  $n = 12$ ,  $\chi = 0.65$ ,  $\chi_{AB} = 0.2$ )

The simulated polymer structures are characterized by a spherical ball of species **B** with species **A** forming various domains on the surface. This trend develops as the block size ratio decreases. Figure 5.2 shows conformations for block size ratios of  $\mathcal{R} = 1$  and  $\mathcal{R} = 0.95$ . When the **A** and **B** blocks are the same

size, a symmetric conformation is formed. However, when the **A** blocks become smaller, the **B** species immediately becomes centralized. The reason for this trend is explained by the theoretical models. (section 3.4)

### 5.3.2 Parameter trends

The simulations are found to follow the trends predicted by the lens model. (section 3.2.3) The following example conformations show the trends as one parameter is varied.

#### Block size ratio

Figure 5.3 shows a sequence of conformations with decreasing block size ratios for otherwise the same polymer chain configuration as in figure 5.2. As the block size ratio decreases, the conformations generally change so that more **A** domains are formed on the surface, as predicted by the lens model.

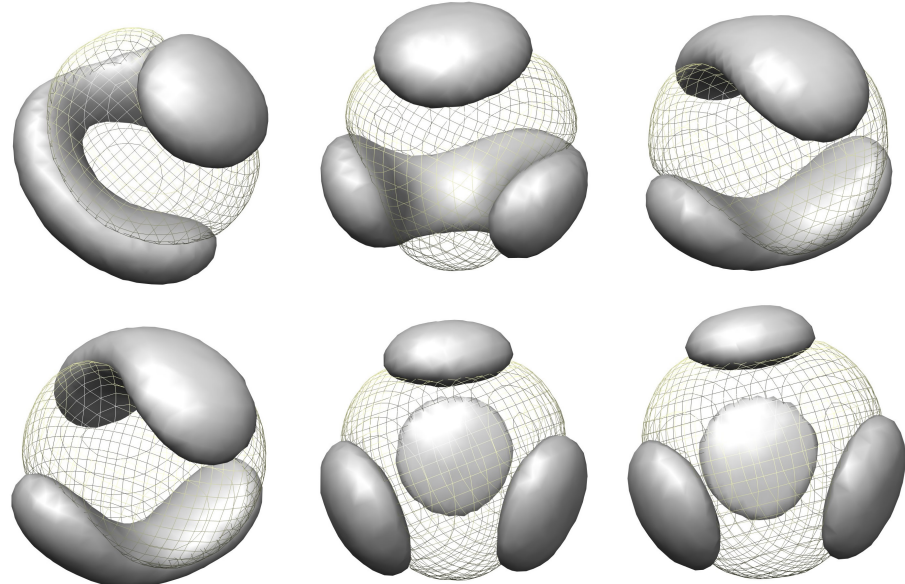


Figure 5.3: Decreasing block size ratio. Top left to right:  $\mathcal{R} = 0.85, 0.75, 0.65$ , and bottom left to right:  $\mathcal{R} = 0.55, 0.45$  and  $0.35$ . The number of **A** domains generally increases as the ratio decreases. (Polymer configuration:  $N = 5520$ ,  $n = 12$ ,  $\chi = 0.65$ ,  $\chi_{AB} = 0.2$ )

### Trend with $\chi$

Figure 5.4 shows a sequence of conformations with increasing  $\chi$  values from left to right. As predicted by the lens model, the number of **A** domains decreases as  $\chi$  increases. The increase in density with  $\chi$  results in an increase in the surface tension free energy. However, there is another factor not accounted for in the lens model which also causes the number of **A** domains to decrease. As  $\chi$  increases, the bulk polymer shape becomes more like a sphere, and the **A** species can protrude less off the surface of the **B** sphere. The **A** domains are forced to spread a little on the surface, moving them closer to neighboring **A** domains. They can then connect more easily, giving a lower number of surface **A** domains.

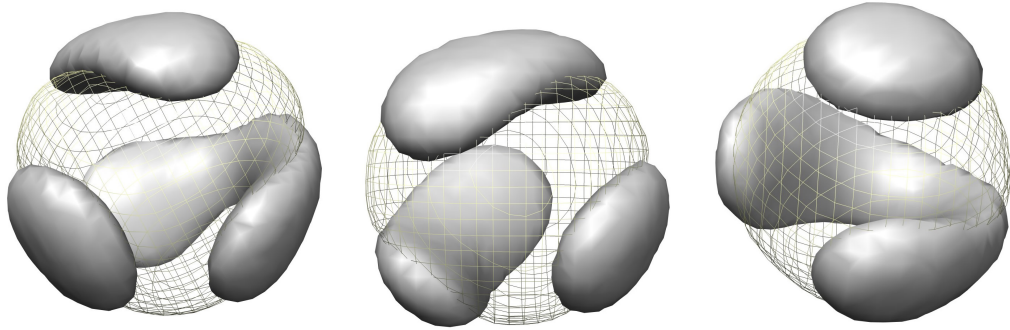


Figure 5.4: Increasing  $\chi$  from left to right:  $\chi = 0.65, 0.7$  and  $0.75$ . In general the number of **A** domains decreases as  $\chi$  increases, although this trend is not as strong as in the block size ratio case. (Polymer configuration:  $N = 6000$ ,  $n = 16$ ,  $\mathcal{R} = 0.5$ ,  $\chi_{AB} = 0.2$ )

The trends with  $N$ ,  $n$  and  $\chi_{AB}$  are more difficult to show with examples. In general these followed the predictions of the model. Figure 5.5 shows conformations with an increasing number of **A** domains for a range of polymer configurations. The clearest trend in these conformations is the increase in **A** domains with number of blocks.

The configurations with low block number  $n$  ( $n = 4 - 8$ ) generally give similar conformations for a large range of  $\chi$ ,  $\chi_{AB}$  and  $\mathcal{R}$  values. This is because the number of **A** blocks heavily limits the number of **A** domains able to form. Most simulations are done on systems with  $n$  above 12 and up to 24, as this gave more interesting results.

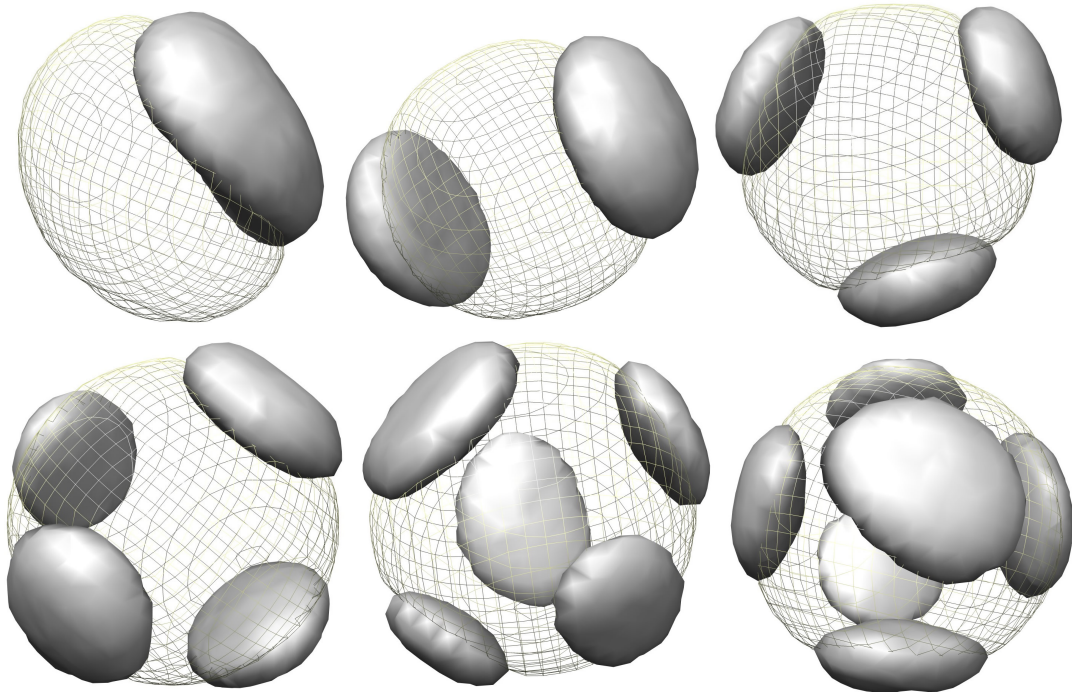


Figure 5.5: SCFT simulation images for conformations with different numbers of **A** domains. The polymer configurations are given in Table 5.1.

Table 5.1: Polymer configuration parameters for Figure 5.5

Conformation	Number of <b>A</b> domains	$N$	$n$	$\mathcal{R}$	$\chi$	$\chi_{AB}$
Top left	1	3840	8	0.4	0.75	0.25
Top middle	2	3840	8	0.4	0.7	0.3
Top right	3	5520	12	0.3	0.7	0.3
Bottom left	4	8192	16	0.3	0.7	0.3
Bottom middle	5	8600	20	0.25	0.7	0.25
Bottom right	6	9600	24	0.35	0.7	0.15

## 5.4 Comparison to the Lens Model

For each simulation run, the number of **A** domains is compared to the number predicted by the lens model (chapter 3). As explained in section 5.1, only those conformations that are judged to have reached equilibrium are included in the

comparison. Figure 5.6 plots the number of **A** domains given by the simulations (simulation value) on the x-axis against the decimal number of **A** domains pre-

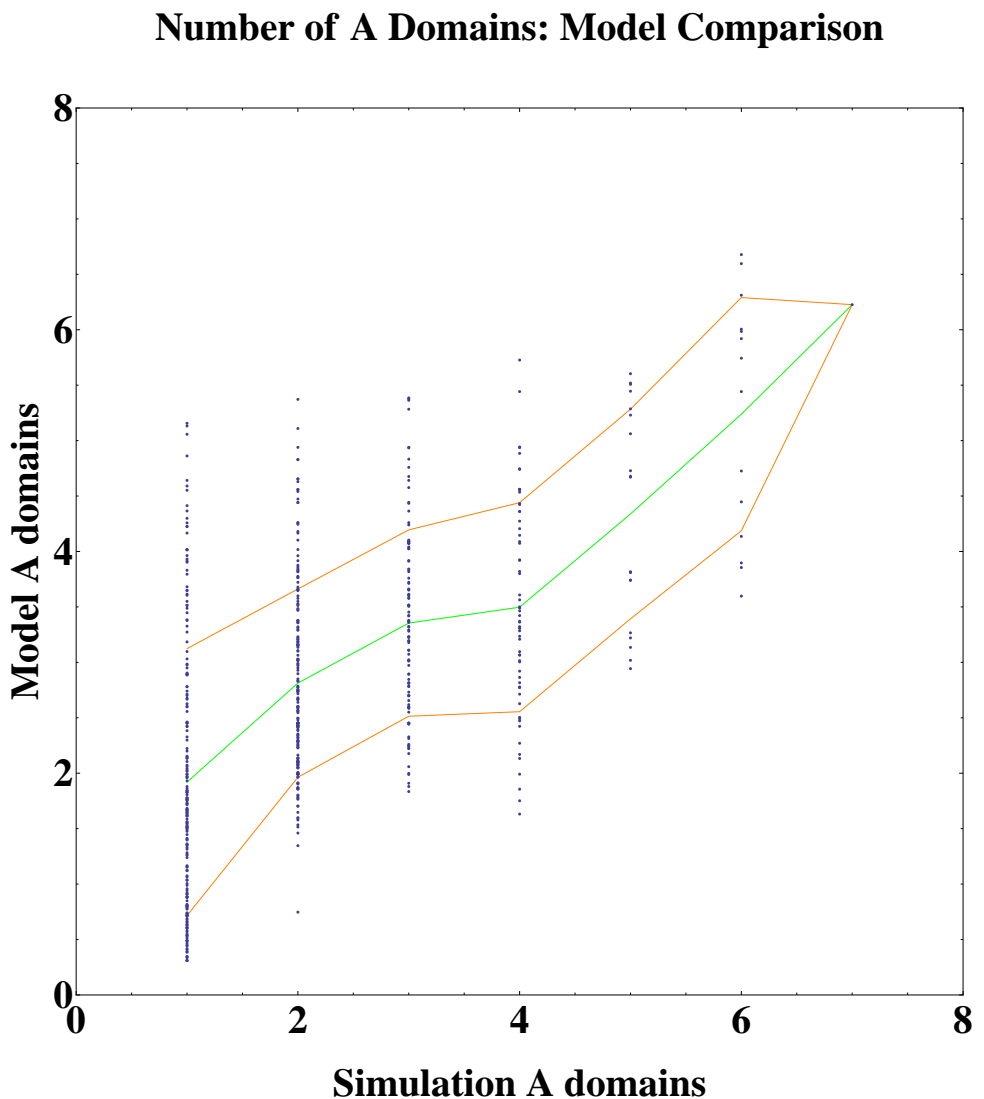


Figure 5.6: **A** domains shown in the simulations versus that predicted by the lens model for the corresponding polymer chain configuration. The green line shows the average at each simulation **A** domain number. The orange lines show the  $1\sigma$  confidence ranges (68% confidence). All valid simulation data is included. Fitting constant = 2.2. The large spread is due mainly to *long ring* conformations produced by the simulations that are not modeled well by the lens model.

dicted by the lens model for the corresponding polymer chain configuration. The decimal model prediction corresponds to the lens size  $x$  in the model such that the free energy is a minimum. This is not converted to an integer lens number in order to make the model-simulation comparison clearer.

If the number of **A** domains from the simulations and the model predictions coincided, then the data would simply be a straight line of slope one. Clearly this is not the case, there is a large spread in the model predicted values for each simulation value. This spread is most pronounced for the simulation value of 1 **A** domain. Many of the simulations do not look like a series of lenses. Instead a range of contorted rings and sausage like shapes are seen, as in figure 5.7 and figure 5.3. The lens model does not model these kinds of conformations well.

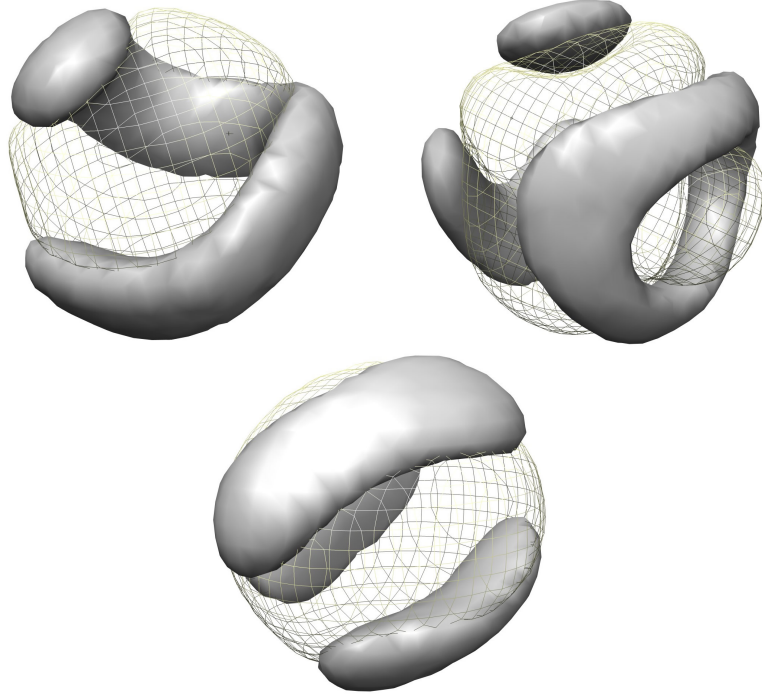


Figure 5.7: Contorted ring conformations not similar to the lens model. Polymer chains forming such conformations are not well modeled by the lens model.

To further test the model, simulation results containing these kinds of rings are removed from the data set. This included any simulation results that contained a *long rail* stretching more than a third of the way around the structure. The resulting data set is shown in figure 5.8.

The fit is now better. In particular, most of the data points with a simulation value of 1 **A** domain and a model prediction of more than 2 **A** domains have been

### Number of A Domains: Model Comparison

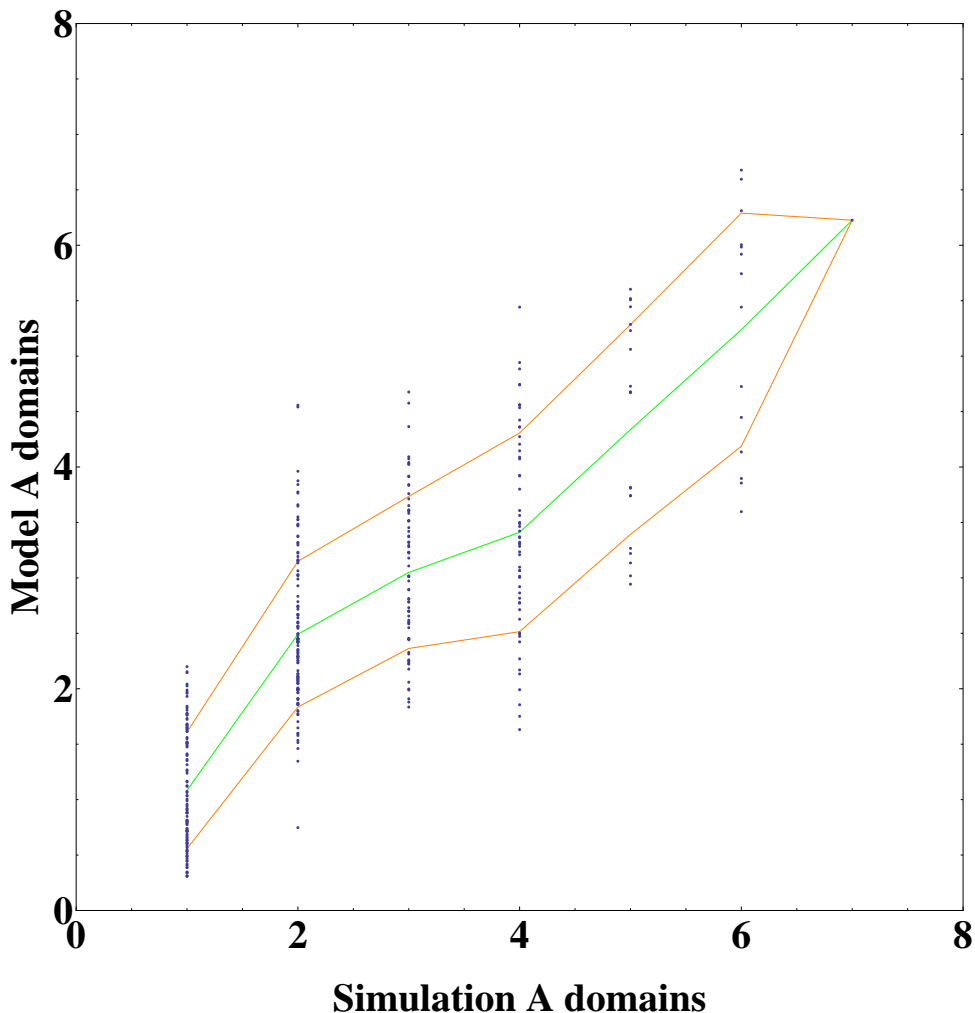


Figure 5.8: **A** domains shown in the simulations versus that predicted by the lens model for the corresponding polymer chain configuration. Conformations clearly not modeled by the lens model are removed. The green line shows the average at each simulation **A** domain number. The orange lines show the  $1\ \sigma$  confidence ranges (68% confidence). Simulation results that contained a long rail that stretched more than a third of the way round the sphere are not included. Fitting constant = 2.2. The spread is now less than in figure 5.6, especially for the simulation value of 1 **A** domain.

removed. These removed simulations are contorted ring conformations similar to the first conformation in figure 5.7. Some outliers from the higher simulation values have also been removed. These conformations had a long ring or rail. The lens model prediction would split such a rail or ring into two or more sections, and a higher **A** domain prediction would result. The main parameter characteristic of the polymer configurations resulting in these conformations is a relatively high block size ratio of 0.5-0.7. This indicates that the lens model works well only for the more asymmetric copolymers.

There is still a large spread, especially for the simulation value of 4 **A** domains. Many of the remaining outliers are technically impossible conformations, given the polymer chain configuration.

## 5.5 Result Validity

Some conformations produced by the simulations appear to be impossible. For example, the *3-stack* conformation shown in figure 5.9 has two *equal sized* **A** surface balls. The volumes of the two **A** balls are almost equal:  $V_{\text{top}} = 0.00354$  and  $V_{\text{bot}} = 0.00397$ . (At surface density display level 0.15)

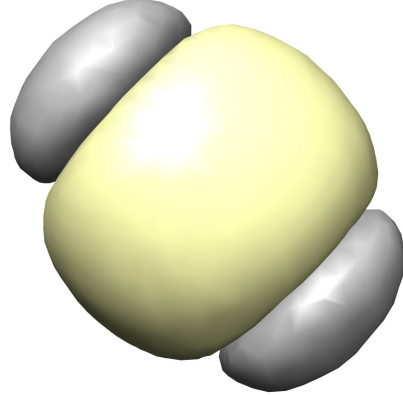


Figure 5.9: A 3-stack conformation  $N = 1890$ ,  $n = 6$ ,  $\mathcal{R} = 0.4$ ,  $\chi = 0.7$ ,  $\chi_{AB} = 0.25$  (surface density = 0.15). The two grey **A** species balls have the same size. This should not be possible since there are only 3 **A** blocks.

This conformation cannot be physically possible when the configuration of the polymer chain is considered. There are three species **A** blocks and hence a physical polymer forming a 3-stack conformation must have different sized balls, one containing two **A** blocks and the other one **A** block. The only way that the

physical polymer can form a conformation where the balls are the same size is if one of the **A** blocks stretches from the top ball to the bottom ball. This would have a very large free-energy cost and is unlikely. There is no evidence of this occurring in the simulation.

The existence of these impossible conformations is due to the statistical nature of the SCFT simulations. The simulation works by propagating *every possible* polymer chain starting at every possible point through space and giving each possible chain state a weighting according to the mean potential (see figure 4.1). A chain state that has an **A** block in a **B**-rich density region will be given a small weighting. A polymer chain state with the **A** and **B** blocks in the correct density regions will be given a large weighting. The polymer conformation is then obtained by doing a weighted average over all the chain states, given their particular weighting factor. The outputted conformations are therefore superpositions of many chain arrangements. The 3-stack conformation could be due to the super-position of polymer chain states having one, two or three blocks in the upper ball with states of the opposite arrangement. (see figure 5.10)

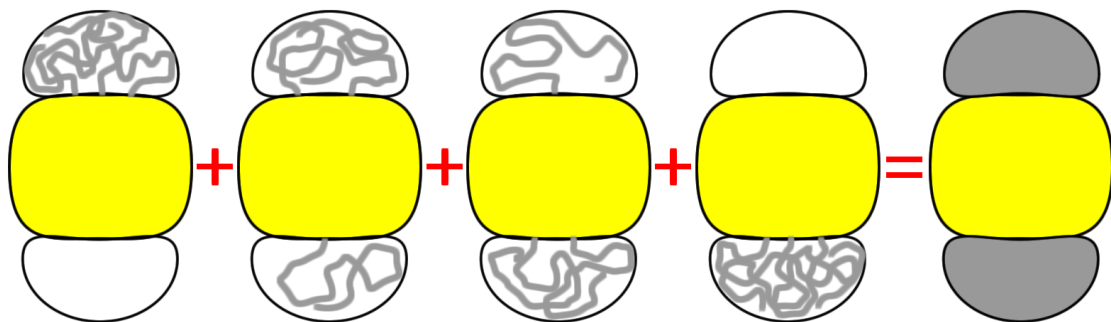


Figure 5.10: Possible polymer chain states contributing to the density field of the 3-stack. The grey blocks only propagate (with significant weighting) in the grey density regions, so this figure shows all the possible arrangements of grey blocks. Each individual chain state gives a conformation that is not symmetric with respect to the upper and lower ball sizes. The sum of all states is however symmetric, with two equal sized **A** balls.

Figure 5.11 shows the density of blocks 1, 3 and 5 for the 3-stack simulation result shown in figure 5.9. The density of each block is split into two sections, which is clearly impossible for a physical polymer. The individual block density conformations result from a superposition of chain states where the block is in

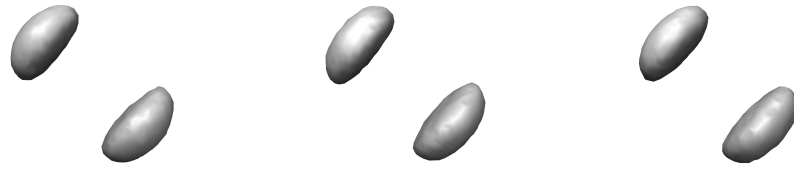


Figure 5.11: Density fields of blocks 1, 3 and 5 for the 3-stack conformation shown in Figure 5.9 (surface density = 0.05). Physically, it should be impossible for these blocks to be split into two separate regions.

either the top or bottom ball.

Other examples of impossible conformations are shown in figure 5.12. The correct physical polymer conformation cannot be extracted from these simulation results simply by taking the most contributing chain state in the averaging process. The superpositions of the other states directly affect the density field, and there is no guarantee that the physical polymer chain would form such a conformation.

It is difficult to resolve this statistical issue, section 5.7 discusses some attempted solutions.

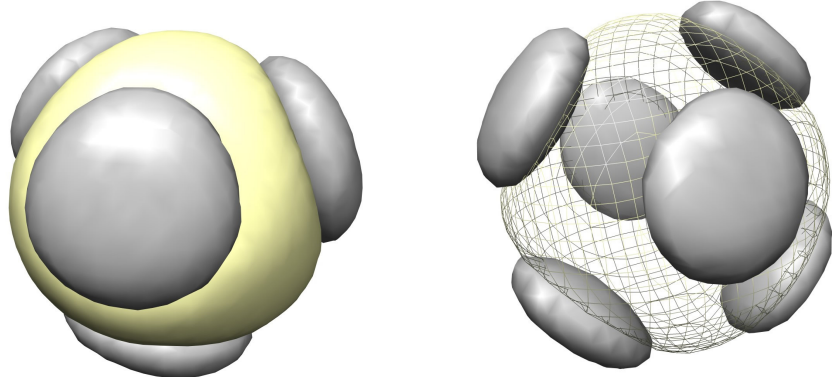


Figure 5.12: (Left) An impossible 4-equal-ball conformation resulting from a 12 block polymer with only 6 **A** blocks. (Right) An impossible 6-equal-ball conformation resulting from a 18 block polymer with only 9 **A** blocks

## 5.6 Model Comparison (Valid Conformations Only)

Any conformations known to be impossible, such as the 4-equal-ball and equal-3-stack conformations shown above, are eliminated from the data. The results after

this elimination are shown in figure 5.13.

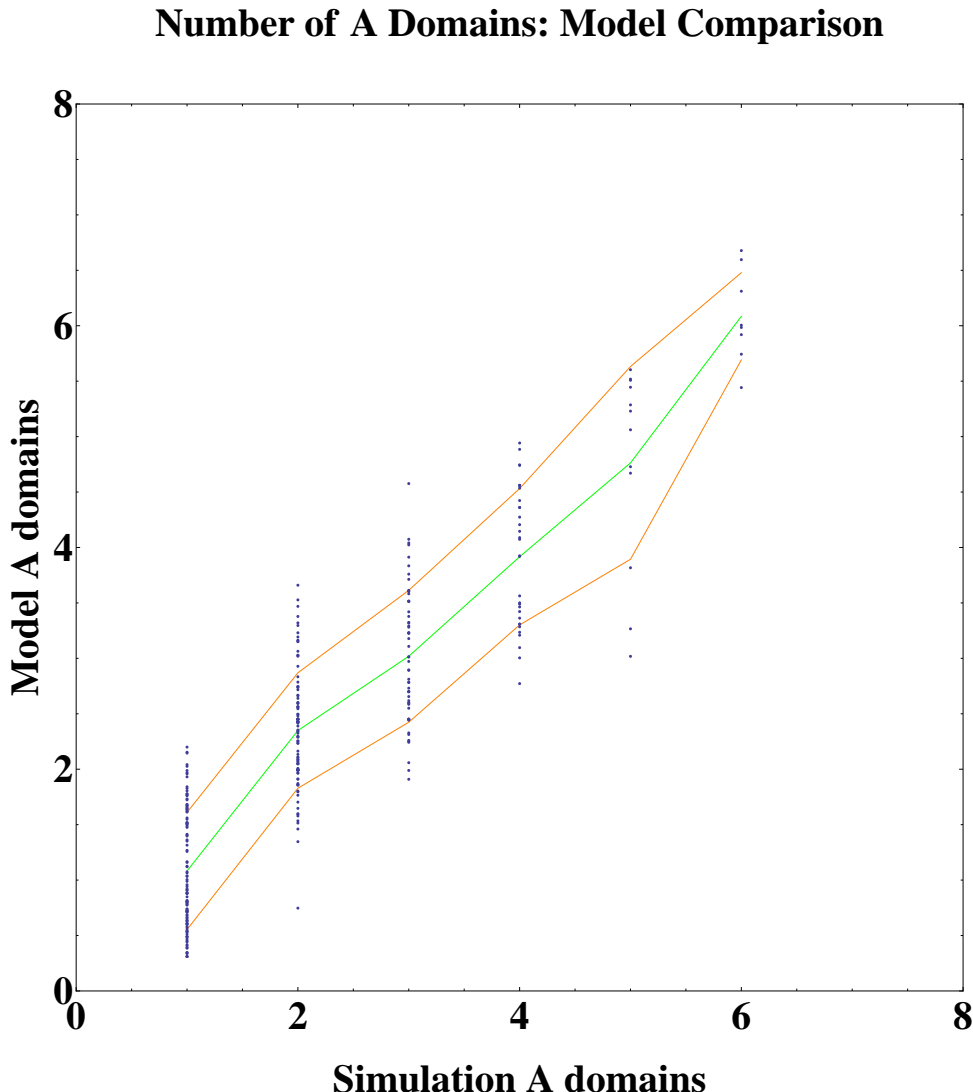


Figure 5.13: **A** domains shown in the simulations versus that predicted by the lens model for the corresponding polymer chain configuration. Any conformations known to be impossible are eliminated. The green line shows the average at each simulation **A** domain number. The orange lines show the  $1\sigma$  confidence ranges (68% confidence). Fitting constant = 2.2. The fit between the model and the simulations now approximately describes a one-to-one relationship with error bars  $\pm 0.5$ .

The correlation is now better. The average **A** domain line approximately describes a one-to-one relationship, after adjusting the fitting parameter within the lens model to 2.2. The standard deviation is approximately 0.5 for most simulation values. This is a small spread in light of the uncertainty sources in the comparison:

- The inaccuracies in the model, including the spherical assumption. (see section 3.2)
- Some of the simulation results may be trapped in semi-stable conformations. These are eliminated where possible by checking the free energy of identical runs, but not every polymer chain was simulated more than once.
- The model can predict an impossible arrangement of blocks, with each lens containing a non-integer number of blocks.

In conclusion, the lens model works well when impossible conformations and conformations containing long rings are eliminated. Since the majority of the long rings appear only for polymer chain configurations with high block size ratios, the model predicts the conformations of highly asymmetric polymer configurations well. The approximate fitting parameter that gives a one-to-one relationship between the lens model and the simulation results is 2.2. This fitting parameter controls the magnitude of the stretching terms in the lens model. So the stretching energy is underestimated by the simple ideal chain stretching in the model by a factor of 2.

The agreement between the simulations and the theoretical lens model for highly asymmetric block copolymers in poor solvents show that an understanding of the polymer system has been reached. The theoretical model explains why many of these conformations are formed. Using both the simulations and model it is now possible to accurately predict the conformations formed by asymmetric block copolymers in poor solvents.

## 5.7 Possible Solutions to the Statistical Problem

### 5.7.1 Hard sphere

It is inherently difficult to stop impossible conformations from appearing in the simulation results while still allowing the simulation to remain free of artificial effects.

One possible solution is to introduce a *hard sphere* potential into the mean potential. Physically, each **A** block should be localized in a relatively small region due to the poor solvent and free energy penalty for stretching. So a potential

acting on the block which is zero within a sphere (of radius  $R_s$ ) surrounding the block should not affect the physical polymer at all. If this potential is very large outside of  $R_s$ , then the the block cannot have a density contribution outside the sphere. The block is effectively forced into one of its *possible* locations (figure 5.11). The key point about this potential is that the block is still completely free to move. It can move around inside the hard sphere potential and since the hard sphere potential is centered on the blocks center of mass, the block is free to move anywhere inside the lattice.

In practice, this method is difficult to implement. It does not work for the higher ratio polymer configurations where the conformation has large contorted rings containing many blocks. In this case each block expands within the rings to fill the hard sphere radius, and hence the result is artificial, dependent on the sphere radius.

For low block size ratio polymer configurations, the size of the sphere is difficult to optimize. It has to be small to prevent blocks overlapping between different **A** domains, but large enough not to affect the shape of the individual block. This range is small, and heavily dependent on the polymer chain configuration. Hence it is impractical to use this method as a solution.

### 5.7.2 A block interaction

Another possible solution is to introduce an interaction  $\chi_{bl}$  between the different **A** blocks. This interaction would serve to separate the blocks, meaning the individual blocks would exist in one piece to minimize free energy. If the interaction is small enough, it would have a very small effect on the actual conformation formed.

This is again difficult to implement. If  $\chi_{bl}$  is too small, then the blocks do not separate. If  $\chi_{bl}$  is too large, then the simulation is just modeling a polymer configuration where each **A** block is a different species. In the mid-range, it is difficult to get the overall polymer density field to collapse. This option proved an impractical solution to the problem.

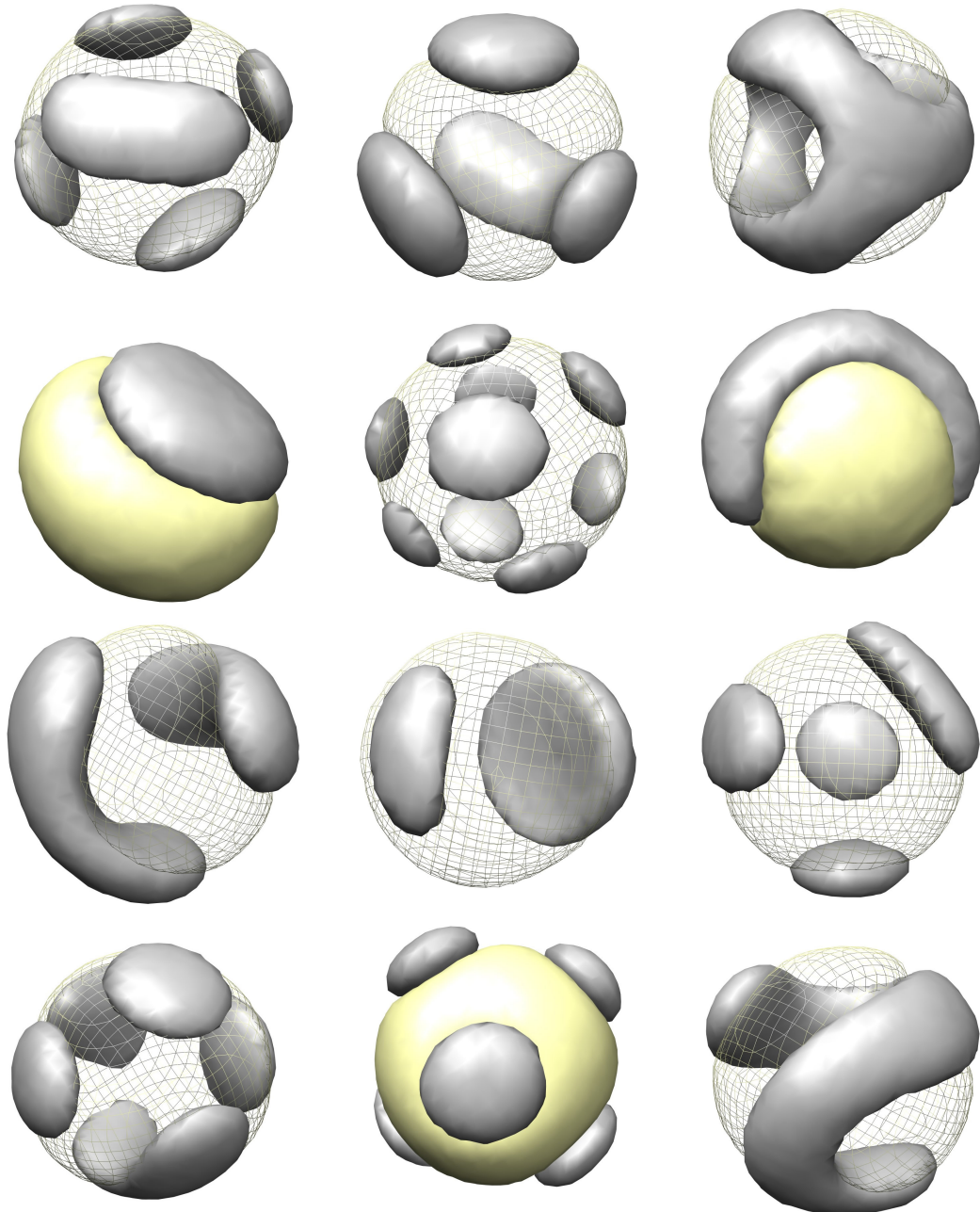


Figure 5.14: Sample SCFT polymer conformation images.

# Chapter 6

## Conclusion and Summary

This thesis investigated the properties of single asymmetric block copolymer chains in poor solvents where the blocks of one species (**A**) are significantly shorter than the blocks of the other species (**B**). In general, it was found that the polymer chain collapses into an approximately spherical globule with species **A** forming a number of surface domains surrounding a species **B** core.

A theoretical free energy model referred to as the *lens model* was developed to predict the number of surface **A** domains formed for different chain configurations. The model gave the trend of number of **A** domains under changes of the five polymer configurational parameters: the number of monomers  $N$ , number of blocks  $n$ , polymer-solvent interaction strength  $\chi$ , polymer-polymer interaction strength  $\chi_{AB}$  and block size ratio  $\mathcal{R} = \frac{N_A}{N_B}$ . The model predicted a decrease in number of **A** domains when  $N$ ,  $\chi$ ,  $\chi_{AB}$  and  $\mathcal{R}$  increased, and an increase in **A** domains with increasing  $n$ .

The lens model was compared to a very different model where species **A** forms a sphere in the *center* of species **B** (the *micelle model*). The lens model gave a lower free energy in the vast majority of cases, as in general it reduced the surface tension free energy. In the extreme case of high monomer number, high  $\chi$ , small block size ratio, high number of blocks and high  $\chi_{AB}$ , this comparison predicted a possible inversion, where the micelle model became the model with a lower free energy. It was not possible to run simulations in this extreme parameter range, but if the simulation method could be improved, it would be interesting to investigate this possible conformation inversion.

The copolymer systems were simulated using *self consistent field theory*. This simulation method was optimized for use with single chain polymers, and the stability was improved. A problem due to the statistical aspect of the method was identified. Often the results produced were impossible, given the structure of the polymer chain. This problem was difficult to solve as it is inherent to the simulation method.

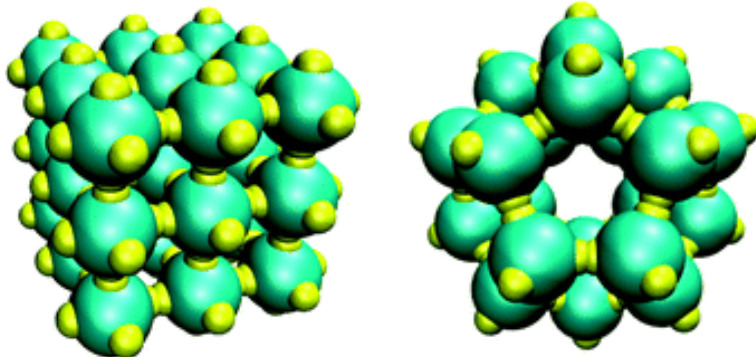


Figure 6.1: Micro-structures formed from patchy colloid self-assembly. source [7]

The predictions of the lens model were compared to the SCFT simulation results. When impossible conformations and conformations resulting from weakly asymmetric polymer chains were removed, the correspondence between model and simulations was good. The fitting parameter used to fit the model to the simulations indicated that the stretching energy in the model was underestimated by a factor of 2.

The results presented in this thesis show that single chain block copolymers can form a diverse range of conformations. For asymmetric block copolymers, an understanding of the polymer system has been obtained. Given an asymmetric block copolymer configuration, it is now possible to predict the conformation formed when the polymer is placed in a poor solvent.

The investigation performed in this thesis shows the potential of block copolymers to form patchy colloid like particles. Patchy colloids are small particles that have surface patches or ‘sticky’ spots that can interact to form complex micrometer size structures. This thesis shows that asymmetric block copolymers in poor solvents could be used as patchy colloid like particles, due to their tendency to form small **A** domains on the surface of a **B** sphere. The **A** domains constitute the patches on the colloids surface, and their number can now be determined from the polymer configuration.

Patchy colloid like particles formed from block copolymers would have many advantages over normal patchy colloids. Their size is significantly smaller (order of 10’s of nanometers) allowing the construction of smaller nano-structures. Block copolymers are easier to make, since they self-assemble when placed in the correct environment. Their structures can also be controlled more easily by changing the polymer configuration and environmental parameters such as temperature and solvent quality, as shown in this thesis.

## 6.1 Further Directions

The methods introduced in this thesis could be easily extended to investigate more complex polymer configurations involving selective solvents, branch points, larger numbers of species and chain stiffness.

The stretching of a polymer chain is another area that could be investigated using SCFT. Computer simulations on polymer stretching have been performed using Langevin dynamics and Monte Carlo simulation techniques [12, 9, 1]. However, SCFT has the ability to converge much more rapidly to the equilibrium conformation of the stretched polymer. The simulations can also be performed on much more complex polymer chains with different block numbers, sizes and species.

As SCFT only finds the equilibrium conformation, no information on the dynamics of the polymer while it is being stretched can be extracted. However, due to the free-energy calculation, the force applied to stretch the polymer at certain stretching distances can be calculated.

A simple feasibility test was done by varying stretching lengths and running the simulation on a 1890 monomer 6 block polymer chain. The results are shown in figure 6.2.

## 6.2 Outcome Summary

The outcomes of this thesis were:

- The development of self consistent field theory simulations for use in simulating single-chain polymers in poor solvents.
- The development of a simple free energy model able to predict the conformation formed by single asymmetric block copolymer chains in poor solvents.
- An understanding of the general conformation formed; The smaller species forms surface domains surrounding a sphere of the larger species.
- The ability to predict the the number of surface domains formed for various polymer configurations.
- The possibility for block copolymers to form patchy colloid like nano-particles, and the ability to control their structure.

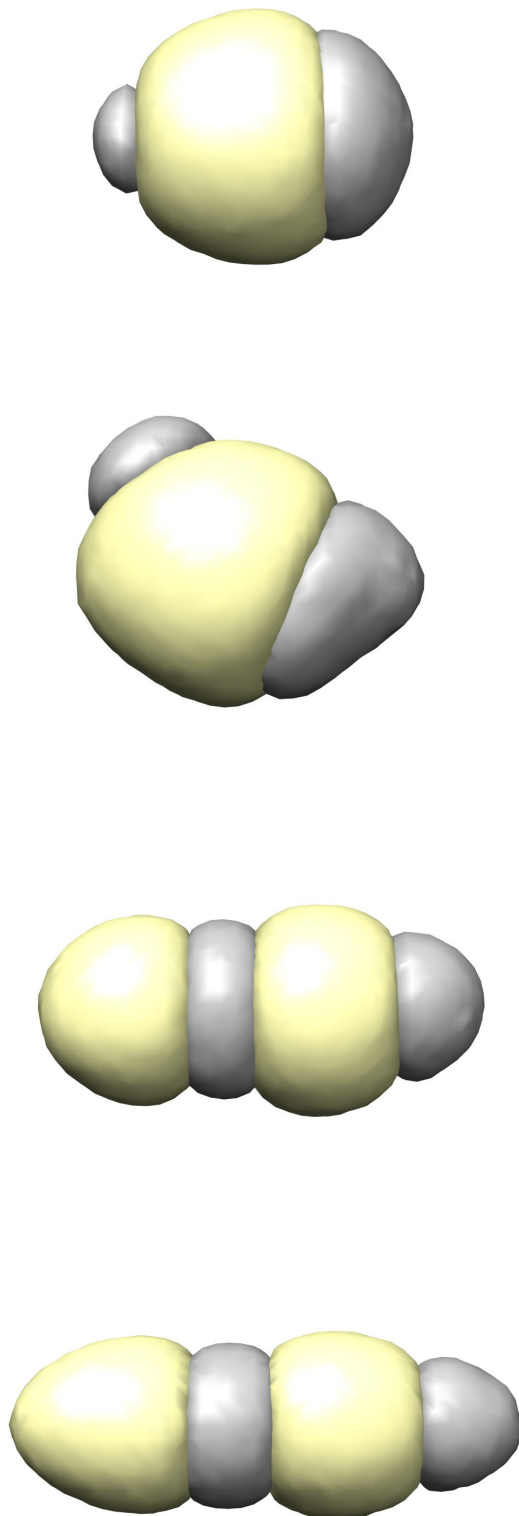


Figure 6.2: A sequence of stretched 6 block polymers at stretching lengths 6,10,14 and 18. Configuration:  $\chi_{AB} = 0.25$ ,  $\chi = 0.7$ ,  $\mathcal{R} = 0.4$ ,  $N = 1890$ ,  $n = 6$ .

# Bibliography

- [1] I R Cooke and D R M Williams, *Stretching polymers in poor and bad solvents: Pullout peaks and an unraveling transition*, Europhysics Letters **64** (2003), no. 2, 267–273.
- [2] A Craig and EM Terentjev, *Stretching globular polymers. I. Single chains*, Journal of Chemical Physics **122** (2005), no. 19.
- [3] P-G de Gennes, *Scaling concepts in polymer physics*, Cornell University Press Ltd., London, UK, 1979.
- [4] KA Dill, SB Ozkan, MS Shell, and TR Weikl, *The protein folding problem*, Annual Review of Biophysics **37** (2008), 289–316.
- [5] C M Dobson, *Protein folding and misfolding*, Nature **426** (2003), no. 6968, 884–890.
- [6] M Doi and S F Edwards, *The theory of polymer dynamics*, Oxford University Press, New York, USA, 1986.
- [7] JPK Doye, AA Louis, I-C Lin, LR Allen, EG Noya, AW Wilber, HC Kok, and R Lyus, *Controlling crystallization and its absence: proteins, colloids and patchy models*, Physical Chemistry Chemical Physics **9** (2007), no. 18, 2197–2205.
- [8] F Drolet and GH Fredrickson, *Optimizing chain bridging in complex block copolymers*, Macromolecules **34** (2001), no. 15, 5317–5324.
- [9] S A Edwards and D R M Williams, *Stretching a single diblock copolymer in a selective solvent: Langevin dynamics simulations*, Macromolecules **38** (2005), no. 25, 10590–10595.
- [10] GH Fredrickson, V Ganesan, and F Drolet, *Field-theoretic computer simulation methods for polymers and complex fluids*, Macromolecules **35** (2002), no. 1, 16–39.

- [11] V Ganesan and GH Fredrickson, *Field-theoretic polymer simulations*, Euro-physics Letters **55** (2001), no. 6, 814–820.
- [12] P Grassberger and H-P Hsu, *Stretched polymers in a poor solvent*, Phys. Rev. E **65** (2002), no. 3, 031807.
- [13] E Helfand and Y Tagami, *Theory of interface between immiscible polymers*, J. Polym. Sci. Part B **9** (1971), no. 10, 741–746.
- [14] P-Y Lai, *Unwinding a polymer in a poor solvent*, Phys. Rev. E **53** (1996), no. 4, 3819–3822.
- [15] N Laurendeau, *Statistical thermodynamics: Fundamentals and applications*, Cambridge University Press, New York, USA, 2005.
- [16] IM Lifshitz and AY Grosberg, *State diagram of a polymer globule and the problem of self-organization of its spatial structure*, Sov. Phys.-JETP (1974), no. 38, 1198–1208.
- [17] IM Lifshitz, AY Grosberg, and AR Khokhlov, *Some problems of statistical physics of polymer-chains with volume interaction*, Reviews of Modern Physics **50** (1978), no. 3, 683–713.
- [18] M. W. Matsen and M. Schick, *Stable and unstable phases of a diblock copolymer melt*, Phys. Rev. Lett. **72** (1994), no. 16, 2660–2663.
- [19] MW Matsen, *The standard Gaussian model for block copolymer melts*, Journal of Physics-Condensed Matter **14** (2002), no. 2, R21–R47.
- [20] DJ Meier, *Theory of block copolymers. i. domain formation in a-b block copolymers*, J. Polym. Sci. Part C **26** (1969), 81–98.
- [21] Regents of the University of California, *UCSF chimera*, 2008.
- [22] T Ohta and K Kawasaki, *Equilibrium morphology of block copolymer melts*, Macromolecules **19** (1986), no. 10, 2621–2632.
- [23] DW Pack, AS Hoffman, S Pun, and PS Stayton, *Design and development of polymers for gene delivery*, Nature Reviews Drug Discovery **4** (2005), no. 7, 581–593.
- [24] C Park, J Yoon, and EL Thomas, *Enabling nanotechnology with self assembled block copolymer patterns*, Polymer **44** (2003), no. 22, 6725–6760.

- [25] DF Parsons and DRM Williams, *Single chains of block copolymers in poor solvents: Handshake, spiral, and lamellar globules formed by geometric frustration*, Physical Review Letters **99** (2007), no. 22.
- [26] SK Pappanayek, TT Pham, and GG Pereira, *Morphological structures formed by grafted polymers in poor solvents*, Journal of Chemical Physics **122** (2005), no. 21.
- [27] MB Pinson and DRM Williams, *Globular states of multi-block copolymer chains in poor solvents: Labyrinthine configurations and the phase diagram*, (2008), Not yet published.
- [28] KO Rasmussen and G Kalosakas, *Improved numerical algorithm for exploring block copolymer mesophases*, Journal of Polymer Science part B-Polymer Physics **40** (2002), no. 16, 1777–1783.
- [29] J Rodriguez-Hernandez, F Checot, Y Gnanou, and S Lecommandoux, *Toward ‘smart’ nano-objects by self-assembly of block copolymers in solution*, Progress in Polymer Science **30** (2005), no. 7, 691–724.
- [30] AV Ruzette and L Leibler, *Block copolymers in tomorrow’s plastics*, Nature Materials **4** (2005), no. 1, 19–31.
- [31] School Computer Unit, Research School of Physical Sciences, the Australian National University.
- [32] A N Semenov, *Contribution to the theory of microphase layering in block-copolymer melts*, Sov. Phys. JETP **61** (1985), 733–742.
- [33] M Suzuki, *Convergence of exponential operators - zassenhaus formula, bch formula and systematic approximants*, Commun. Math. Phys. **57** (1977), no. 3, 193–200.
- [34] RB Thompson, VV Ginzburg, MW Matsen, and AC Balazs, *Block copolymer-directed assembly of nanoparticles: Forming mesoscopically ordered hybrid materials*, Macromolecules **35** (2002), no. 3, 1060–1071.
- [35] RB Thompson, KO Rasmussen, and T Lookman, *Improved convergence in block copolymer self-consistent field theory by Anderson mixing*, Journal of Chemical Physics **120** (2004), no. 1, 31–34.
- [36] A van Blaaderen, *Materials science - Colloids get complex*, Nature **439** (2006), no. 7076, 545–546.

- [37] RM Wilcox, *Exponential operators and parameter differentiation in quantum physics*, Journal of Mathematical Physics **8** (1967), no. 4, 962–982.
- [38] C Williams, F Brochard, and HL Frisch, *Polymer collapse*, Annual Review of Physical Chemistry **32** (1981), 433–451.

# Chapter 7

## Appendix 1: The Solution to the Propagator Equation

### 7.1 Mean Field Formula

The formulas for the mean fields  $w_A$  and  $w_B$  are obtained by minimizing the free energy in the density field representation with respect to  $\phi_A$  and  $\phi_B$ . The free energy is (2.6):

$$F = -\log \int_V q(\mathbf{r}, N) d\mathbf{r} + \int_V [\phi_S \log(\phi_S) + \chi (\phi_A \phi_S + \phi_B \phi_S) + \chi_{AB} \phi_A \phi_B] d\mathbf{r}$$

Taking the derivative with respect to  $\phi_A$ :

$$\begin{aligned} \frac{\partial F}{\partial \phi_A} &= \int \frac{\partial}{\partial \phi_A} \left[ (1 - \phi_A - \phi_B) \log(1 - \phi_A - \phi_B) + \chi \phi_A \phi_S \right. \\ &\quad \left. + \chi \phi_B \phi_S + \chi_{AB} \phi_A \phi_B - w_A \phi_A - w_B \phi_B \right] d\mathbf{r} \\ &= \int \left[ -\log(1 - \phi_A - \phi_B) + 1 - 1 + \chi(1 - 2\phi_A - \phi_B) - \chi \phi_B \right. \\ &\quad \left. + \chi_{AB} \phi_B - w_A \right] d\mathbf{r} + C \\ &= \int \left[ \chi(1 - 2\phi_A) + (\chi_{AB} - 2\chi) \phi_B - \log(1 - \phi_A - \phi_B) - w_A \right] d\mathbf{r} + C \end{aligned}$$

So ignoring constants, setting to zero and rearranging:

$$w_A(\mathbf{r}) = \chi_{AS}(1 - 2\phi_A) + (\chi_{AB} - \chi_{AS} - \chi_{BS})\phi_B - \log(1 - \phi_A - \phi_B)$$

and similarly for  $w_B$ :

$$w_B(\mathbf{r}) = \chi_{BS}(1 - 2\phi_B) + (\chi_{AB} - \chi_{AS} - \chi_{BS})\phi_A - \log(1 - \phi_A - \phi_B)$$

## 7.2 Solving the Propagator Equation

Most of the computational effort in SCFT goes into solving the propagator equation:

$$\frac{\partial q}{\partial s}(\mathbf{r}, s) = \frac{b^2}{6} \nabla^2 q(\mathbf{r}, s) - w(\mathbf{r})q(\mathbf{r}, s)$$

A formal solution can be obtained through:

$$\begin{aligned} \frac{\partial q}{\partial s}(\mathbf{r}, s) &= \left( \frac{b^2}{6} \nabla^2 - w(\mathbf{r}) \right) q(\mathbf{r}, s) \\ \implies \frac{1}{q} \partial q &= \left( \frac{b^2}{6} \nabla^2 - w \right) \partial s \\ \implies \int_{q(\mathbf{r}, s)}^{q(\mathbf{r}, s + \delta s)} \frac{1}{q} dq &= \int_s^{s + \delta s} \hat{A} ds \\ \implies \log \left( \frac{q(\mathbf{r}, s + \delta s)}{q(\mathbf{r}, s)} \right) &= \hat{A} \delta s \\ \implies q(\mathbf{r}, s + \delta s) &= e^{\hat{A} \delta s} q(\mathbf{r}, s) \end{aligned}$$

So the formal solution is:

$$q(\mathbf{r}, s + \delta s) = \exp \left( \frac{\delta s b^2}{6} \nabla^2 - \delta s w \right) q(\mathbf{r}, s)$$

In order to solve this equation, the exponentials need to be written in a more convenient form. Setting  $A = \frac{b^2}{6} \nabla^2$ ,  $B = -w(\mathbf{r})$  and  $\lambda = \delta s$  the exponential is now in the form  $e^{\lambda(A+B)}$  where  $A$  and  $B$  are non-commuting operators. The exponential needs to be separated into an  $A$  and a  $B$  part. Writing:

$$e^{\lambda(A+B)} = \prod_{n=\infty}^2 e^{\lambda^n C_n} e^{\lambda B} e^{\lambda A} \quad (7.1)$$

(variation of the Zassenhaus Formula [33, 37]). So the coefficients  $C_n$  need to be found to solve the differential equation. They can be defined as:

$$C_n = \frac{1}{n!} \left[ \frac{\partial^n}{\partial \lambda^n} \left( e^{\lambda(A+B)} e^{-\lambda A} e^{-\lambda B} e^{-\lambda^2 C_2} \dots e^{-\lambda^{n-1} C_{n-1}} \right) \right]_{\lambda=0}$$

since substituting in (7.1) gives:

$$\begin{aligned}
C_n &= \frac{1}{n!} \left[ \frac{\partial^n}{\partial \lambda^n} \left( \prod_{m=\infty}^2 e^{\lambda^m C_m} e^{\lambda B} e^{\lambda A} e^{-\lambda A} e^{-\lambda B} e^{-\lambda^2 C_2} \dots e^{-\lambda^{n-1} C_{n-1}} \right) \right]_{\lambda=0} \\
&= \frac{1}{n!} \left[ \frac{\partial^n}{\partial \lambda^n} \left( \prod_{m=\infty}^n e^{\lambda^m C_m} \right) \right]_{\lambda=0} \\
&= \frac{1}{n!} \left[ \prod_{m=\infty}^{n+1} e^{\lambda^m C_m} \frac{\partial^n}{\partial \lambda^n} (e^{\lambda^n C_n}) + \dots \right]_{\lambda=0} \\
&= \frac{1}{n!} \left[ \prod_{m=\infty}^{n+1} e^{\lambda^m C_m} (e^{\lambda^n C_n} n! C_n) + \lambda(\dots) + \lambda^2(\dots) + \dots \right]_{\lambda=0} \\
&= C_n
\end{aligned}$$

### 7.2.1 Finding the coefficients using the Wilcox method

Taking the derivative of both sides of Eq. (7.1) w.r.t  $\lambda$  gives:

$$e^{\lambda(A+B)}(A+B) = \prod_{n=\infty}^2 e^{\lambda^n C_n} e^{\lambda B} e^{\lambda A} A + \prod_{n=\infty}^2 e^{\lambda^n C_n} e^{\lambda B} B e^{\lambda A} + \prod_{n=\infty}^2 e^{\lambda^n C_n} 2\lambda C_2 e^{\lambda B} e^{\lambda A} + \dots$$

multiplying on the left by the reciprocal of (7.1);  $e^{-\lambda(A+B)} = e^{-\lambda A} e^{-\lambda B} \prod_{n=2}^{\infty} e^{-\lambda^n C_n}$  gives:

$$A+B = A + e^{-\lambda A} B e^{\lambda A} + e^{-\lambda A} e^{-\lambda B} 2\lambda C_2 e^{\lambda B} e^{\lambda A} + e^{-\lambda A} e^{-\lambda B} e^{-\lambda^2 C_2} 3\lambda^2 C_3 e^{\lambda^2 C_2} e^{\lambda B} e^{\lambda A} + \dots$$

$$\implies B = e^{-\lambda A} B e^{\lambda A} + e^{-\lambda A} e^{-\lambda B} 2\lambda C_2 e^{\lambda B} e^{\lambda A} + e^{-\lambda A} e^{-\lambda B} e^{-\lambda^2 C_2} 3\lambda^2 C_3 e^{\lambda^2 C_2} e^{\lambda B} e^{\lambda A} + \dots \quad (7.2)$$

Now since  $A = \frac{b^2}{6} \nabla^2$  and  $B = -w(\mathbf{r})$  then:

$$\begin{aligned}
[A, B]f(\mathbf{r}) &= \frac{b^2}{6} \nabla^2(-w \cdot f) + w \cdot \frac{b^2}{6} \nabla^2 f \\
&= -f \cdot \frac{b^2}{6} \nabla^2(w) - w \cdot \frac{b^2}{6} \nabla^2(\cdot f) + w \cdot \frac{b^2}{6} \nabla^2 f \\
&= -\frac{b^2}{6} \nabla^2(w) \cdot f = g(\mathbf{r}) \cdot f \\
\implies [A, B] &= g(\mathbf{r})
\end{aligned}$$

Also, from the explicit formulas for  $C_n$  above:

$$\begin{aligned}
 C_2 &= \frac{1}{2} \left[ \frac{\partial^2}{\partial \lambda^2} \left( e^{\lambda(A+B)} e^{-\lambda A} e^{-\lambda B} \right) \right]_{\lambda=0} \\
 &= \frac{1}{2} \left[ \frac{\partial}{\partial \lambda} \left( e^{\lambda(A+B)} ((A+B)e^{-\lambda A} e^{-\lambda B} - Ae^{-\lambda A} e^{-\lambda B} - e^{-\lambda A} e^{-\lambda B} B) \right) \right]_{\lambda=0} \\
 &= \frac{1}{2} \left[ (A+B) (((A+B) - A - B)) + ((A+B)(-A - B) \right. \\
 &\quad \left. - A(-A - B) - (-A - B)B) \right] \\
 \implies C_2 &= \frac{1}{2}[A, B]
 \end{aligned}$$

$$\begin{aligned}
 C_3 &= \frac{1}{6} \left[ \frac{\partial^3}{\partial \lambda^3} \left( e^{\lambda(A+B)} e^{-\lambda A} e^{-\lambda B} e^{-\lambda^2 C_2} \right) \right]_{\lambda=0} \\
 &= \frac{1}{6} \left[ \frac{\partial^3}{\partial \lambda^3} \left( e^{\lambda(A+B)} e^{-\lambda A} e^{-\lambda B} \right) + \frac{\partial^2}{\partial \lambda^2} \left( e^{\lambda(A+B)} e^{-\lambda A} e^{-\lambda B} \right) (-2\lambda C_2) \right. \\
 &\quad \left. + \frac{\partial}{\partial \lambda} \left( e^{\lambda(A+B)} e^{-\lambda A} e^{-\lambda B} \right) (-2C_2 + 4\lambda^2 C_2^2) + \frac{\partial}{\partial \lambda} \left( (-2C_2 + 4\lambda^2 C_2^2) e^{-\lambda^2 C_2} \right) \right]_{\lambda=0} \\
 &= \frac{1}{6} \left[ \frac{\partial^3}{\partial \lambda^3} \left( e^{\lambda(A+B)} e^{-\lambda A} e^{-\lambda B} \right) + ((A+B) - A - B) (-2C_2) \right]_{\lambda=0} \\
 &= \frac{1}{6} \left[ \frac{\partial^2}{\partial \lambda^2} \left( e^{\lambda(A+B)} ((A+B)e^{-\lambda A} e^{-\lambda B} - Ae^{-\lambda A} e^{-\lambda B} - e^{-\lambda A} e^{-\lambda B} B) \right) \right]_{\lambda=0} \\
 &= \frac{1}{6} \left[ (A+B) \frac{\partial^2}{\partial \lambda^2} \left( e^{\lambda(A+B)} e^{-\lambda A} e^{-\lambda B} \right) - \frac{\partial^2}{\partial \lambda^2} \left( e^{\lambda(A+B)} Ae^{-\lambda A} e^{-\lambda B} \right) \right. \\
 &\quad \left. - \frac{\partial^2}{\partial \lambda^2} \left( e^{\lambda(A+B)} e^{-\lambda A} e^{-\lambda B} \right) B \right]_{\lambda=0} \\
 &= \frac{1}{3} \left[ -\frac{1}{2} \frac{\partial^2}{\partial \lambda^2} \left( e^{\lambda(A+B)} Ae^{-\lambda A} e^{-\lambda B} \right) \right]_{\lambda=0} + \frac{1}{3} ((A+B)C_2 - C_2 B)
 \end{aligned}$$

But  $B$  commutes with  $C_2$  since they are both functions of space. So:

$$\begin{aligned}
C_3 &= \frac{1}{3} \left[ -\frac{1}{2} \frac{\partial}{\partial \lambda} (e^{\lambda(A+B)}(A+B)(Ae^{-\lambda A}e^{-\lambda B}) - e^{\lambda(A+B)}(A^2e^{-\lambda A} + Ae^{-\lambda A}B)e^{-\lambda B}) \right]_{\lambda=0} \\
&\quad + \frac{1}{3} AC_2 \\
&= \frac{1}{3} \left[ -\frac{1}{2} \frac{\partial}{\partial \lambda} (e^{\lambda(A+B)}(BAe^{-\lambda A} - Ae^{-\lambda A}B)e^{-\lambda B}) \right]_{\lambda=0} + \frac{1}{3} AC_2 \\
&= \frac{1}{3} \left[ -\frac{1}{2} ((A+B)(BA - AB) - BA^2 + A^2B - BAB + AB^2) \right] + \frac{1}{3} AC_2 \\
&= \frac{1}{3} \left[ -\frac{1}{2} ([A, B]A + B[B, A] + [A, B]B) \right] + \frac{1}{3} AC_2 \\
&= \frac{1}{3}[A, C_2] = \frac{1}{6}[A, [A, B]]
\end{aligned}$$

So clearly all the  $C_n$ 's involve commutators of  $A$  and  $B$  and are functions of space. So all the  $C_n$ 's commute with each other and with  $B$ . Hence Eq (7.2) becomes:

$$\begin{aligned}
B &= e^{-\lambda A}Be^{\lambda A} + e^{-\lambda A}e^{-\lambda B}2\lambda C_2e^{\lambda B}e^{\lambda A} + e^{-\lambda A}e^{-\lambda B}e^{-\lambda^2 C_2}3\lambda^2 C_3e^{\lambda^2 C_2}e^{\lambda B}e^{\lambda A} + \dots \\
&= e^{-\lambda A}Be^{\lambda A} + e^{-\lambda A}2\lambda C_2e^{\lambda A} + e^{-\lambda A}3\lambda^2 C_3e^{\lambda A} + \dots
\end{aligned}$$

So defining  $C_1 = B$ :

$$B = \sum_{n=1}^{\infty} n\lambda^{n-1}e^{-\lambda A}C_ne^{\lambda A}$$

Now using the identity:

$$e^Y X e^{-Y} = X + [Y, X] + \frac{1}{2}[Y, [Y, X]] + \dots = \sum_{n=0}^{\infty} \frac{1}{n!}[Y, \dots, [Y, X] \dots]^{\neg n}$$

Where the notation  $\neg^n$  indicates that the  $Y$  occurs  $n$  times. Hence:

$$\begin{aligned}
B &= \sum_{n=1}^{\infty} n\lambda^{n-1} \sum_{m=0}^{\infty} \frac{\lambda^m(-1)^m}{m!} [A, \dots, [A, C_n] \dots]^{\neg m} \\
&= \sum_{n=1}^{\infty} \sum_{m=n}^{\infty} \frac{n\lambda^{m-1}(-1)^{m-n}}{(m-n)!} [A, \dots, [A, C_n] \dots]^{\neg m-n} \\
&= \sum_{m=1}^{\infty} \sum_{n=1}^m \frac{n\lambda^{m-1}(-1)^{m-n}}{(m-n)!} [A, \dots, [A, C_n] \dots]^{\neg m-n}
\end{aligned}$$

so equating coefficients of  $\lambda$ , the zeroth order terms give:

$$B = C_1$$

and the  $(m - 1)$ th order terms give:

$$\begin{aligned} 0 &= \sum_{n=1}^m \frac{n(-1)^{m-n}}{(m-n)!} [A, \dots, [A, C_n] \dots]^{\neg m-n} \\ &= \sum_{n=1}^{m-1} \frac{n(-1)^{m-n}}{(m-n)!} [A, \dots, [A, C_n] \dots]^{\neg m-n} + mC_m \\ \implies mC_m &= \sum_{n=1}^{m-1} \frac{n(-1)^{m-n-1}}{(m-n)!} [A, \dots, [A, C_n] \dots]^{\neg m-n} \end{aligned}$$

Now assume a formula for  $C_n$  suggested by the calculations above of  $C_2$  and  $C_3$  and prove it by induction:

$$C_n = \frac{1}{n!} [A, \dots, [A, B] \dots]^{\neg n-1}$$

This is true for  $n = 2, 3$ . Substituting into the above repetition formula (for terms  $n < m$ ):

$$\begin{aligned} mC_m &= \sum_{n=1}^{m-1} \frac{n(-1)^{m-n-1}}{(m-n)!} [A, \dots, [A, (\frac{1}{n!} [A, \dots, [A, B] \dots]^{\neg n-1})] \dots]^{\neg m-n} \\ &= \sum_{n=1}^{m-1} \frac{n(-1)^{m-n-1}}{(m-n)!n!} [A, \dots, [A, B] \dots]^{\neg m-1} \\ &= [A, \dots, [A, B] \dots]^{\neg m-1} \sum_{n=1}^{m-1} \frac{(-1)^{m-n-1}}{(m-n)!(n-1)!} \end{aligned}$$

So the sum term above must be shown to be equal to  $\frac{1}{(m-1)!}$ . To see this consider the binomial expansion of  $(1-x)^{m-1}$ :

$$\begin{aligned} (1-x)^{m-1} &= \sum_{k=0}^{m-1} \binom{m-1}{k} (-x)^{m-1-k} \\ &= \sum_{k=0}^{m-1} \frac{(m-1)!}{k!(m-1-k)!} (-1)^{m-1-k} x^{m-1-k} \end{aligned}$$

let  $n = k + 1$ :

$$\begin{aligned}
 (1-x)^{m-1} &= \sum_{n=1}^m \frac{(m-1)!}{(n-1)!(m-n)!} (-1)^{m-n} x^{m-n} \\
 &= -(m-1)! \left( \sum_{n=1}^m \frac{(-1)^{m-n-1}}{(n-1)!(m-n)!} x^{m-n} \right) \\
 &= -(m-1)! \left( \sum_{n=1}^{m-1} \frac{(-1)^{m-n-1}}{(n-1)!(m-n)!} x^{m-n} - \frac{1}{(m-1)!} \right) \\
 \implies (1-x)^{m-1} &= -(m-1)! \sum_{n=1}^{m-1} \frac{(-1)^{m-n-1}}{(n-1)!(m-n)!} x^{m-n} + 1
 \end{aligned}$$

Choosing  $x = 1$ :

$$\sum_{n=1}^{m-1} \frac{(-1)^{m-n-1}}{(n-1)!(m-n)!} = \frac{1}{(m-1)!}$$

and hence it has been proven by induction that:

$$C_n = \frac{1}{n!} [A, \dots [A, B] \dots]^{\top n-1}$$

Using  $A = \frac{b^2}{6} \nabla^2$  and  $B = -w$ :

$$\begin{aligned}
 C_{n+1} &= \frac{1}{(n+1)!} [A, \dots [A, -\frac{b^2}{6} \nabla^2(w)] \dots]^{\top n-1} \\
 &= -\frac{1}{(n+1)!} \frac{b^{2n}}{6^n} \nabla^{2n}(w)
 \end{aligned}$$

### 7.2.2 Solution in terms of separated exponentials

Using this in the formal equation solution:

$$\begin{aligned}
 q(\mathbf{r}, s + \delta s) &= \prod_{n=\infty}^2 e^{\delta s^n C_n} e^{-\delta s w(\mathbf{r})} \exp \left( \delta s \frac{b^2}{6} \nabla^2 \right) q(\mathbf{r}, s) \\
 &= \prod_{n=\infty}^1 e^{\delta s^{n+1} \left( -\frac{1}{(n+1)!} \frac{b^{2n}}{6^n} \nabla^{2n} w \right)} e^{-\delta s w(\mathbf{r})} \exp \left( \delta s \frac{b^2}{6} \nabla^2 \right) q(\mathbf{r}, s) \\
 &= \left( \prod_{n=\infty}^1 e^{-\frac{\delta s^{n+1} b^{2n}}{6^n (n+1)!} \nabla^{2n} w} e^{-\delta s w(\mathbf{r})} \right) \exp \left( \delta s \frac{b^2}{6} \nabla^2 \right) q(\mathbf{r}, s) \\
 &= \gamma \exp \left( \delta s \frac{b^2}{6} \nabla^2 \right) q(\mathbf{r}, s)
 \end{aligned}$$

Where:

$$\begin{aligned}\gamma &= \prod_{n=\infty}^1 e^{-\frac{\delta s^{n+1} b^{2n}}{6^n(n+1)!} \nabla^{2n} w} e^{-\delta s w(\mathbf{r})} \\ &= \exp \left( -\sum_{n=1}^{\infty} \frac{\delta s^{n+1} b^{2n}}{6^n(n+1)!} \nabla^{2n} w - \delta s w \right) \\ &= \exp \left( -\delta s \sum_{n=0}^{\infty} \frac{\delta s^n b^{2n}}{6^n(n+1)!} \nabla^{2n} w \right)\end{aligned}$$

This coefficient cannot be evaluated because of the infinite sum. It can be approximated by noting:

$$\begin{aligned}\sum_{n=0}^{\infty} \frac{\delta s^n b^{2n}}{6^n(n+1)!} \nabla^{2n} w &= w + \frac{\delta s b^2}{6 \cdot 2} \nabla^2 w + \frac{\delta s^2 b^4}{6^2 \cdot 6} \nabla^4 w + \dots \\ &\approx w + \frac{\delta s b^2}{6 \cdot 2} \nabla^2 w + \frac{\delta s^2 b^4}{6^2 \cdot 8} \nabla^4 w + \dots = \exp \left( \frac{\delta s}{2} \frac{b^2}{6} \nabla^2 \right) w\end{aligned}$$

Which is accurate up to first order. Hence the solution is:

$$\begin{aligned}q(\mathbf{r}, s + \delta s) &= \gamma \exp \left( \delta s \frac{b^2}{6} \nabla^2 \right) q(\mathbf{r}, s) \\ \text{where } \gamma &= \exp \left( -\delta s \exp \left( \frac{\delta s}{2} \frac{b^2}{6} \nabla^2 \right) w \right)\end{aligned}$$

### 7.2.3 Solution of simple diffusion equation

To evaluate this solution the function  $\exp \left( \delta s \frac{b^2}{6} \nabla^2 \right) g(\mathbf{r})$  needs to be found with  $g(\mathbf{r}) = q(\mathbf{r}, s)$  and also with  $\delta s \rightarrow \frac{\delta s}{2}$ ,  $g(\mathbf{r}) = w(\mathbf{r})$ . But this is the solution of the simple diffusion equation (propagator equation without the mean field term):

$$\begin{aligned}\frac{\partial}{\partial t} f(\mathbf{r}, t) &= \frac{b^2}{6} \nabla^2 f(\mathbf{r}, t) \\ \implies \mathcal{L} f(\mathbf{r}, t) &= 0, \quad \mathcal{L} = \frac{b^2}{6} \nabla^2 - \frac{\partial}{\partial t}\end{aligned}$$

Given a known initial condition  $f(\mathbf{r}, 0)$ , the solution to the above equation can be written using a green's function as:

$$f(\mathbf{r}, t) = \int_{allspace} G(\mathbf{r} - \mathbf{r}', t) f(\mathbf{r}', 0) d\mathbf{r}'$$

where  $\mathcal{L}G(\mathbf{r}, t) = 0$ . Using a gaussian form of the green's function:

$$G(\mathbf{r}, t) = \frac{A}{t^{3/2}} \exp\left(-\frac{B|\mathbf{r}|^2}{t}\right)$$

we have:

$$\begin{aligned} \mathcal{L}G(\mathbf{r}, t) &= A \left( \frac{b^2}{6} \nabla^2 - \frac{\partial}{\partial t} \right) \frac{1}{t^{3/2}} \exp\left(-\frac{B|\mathbf{r}|^2}{t}\right) \\ &= A \left[ \frac{b^2}{6t^{3/2}} \left( \frac{\partial^2}{\partial x^2} + \frac{\partial^2}{\partial y^2} + \frac{\partial^2}{\partial z^2} \right) \exp\left(-\frac{B(x^2 + y^2 + z^2)}{t}\right) \right. \\ &\quad \left. - \frac{\partial}{\partial t} \left( \frac{1}{t^{3/2}} \exp\left(-\frac{B|\mathbf{r}|^2}{t}\right) \right) \right] \\ &= A \left[ \frac{b^2}{6t^{3/2}} \left( \frac{\partial}{\partial x} \left( -\frac{2xB}{t} \exp\left(-\frac{B(x^2 + y^2 + z^2)}{t}\right) \right) \right) + \dots \right] \\ &\quad + \left( \frac{3}{2t^{5/2}} - \frac{B|\mathbf{r}|^2}{t^{7/2}} \right) \exp\left(-\frac{B|\mathbf{r}|^2}{t}\right) \\ &= A \left( \frac{b^2}{6t^{3/2}} \left( -\frac{2B}{t} + \frac{4B^2x^2}{t^2} + \dots \right) + \frac{3}{2t^{5/2}} - \frac{B|\mathbf{r}|^2}{t^{7/2}} \right) \exp\left(-\frac{B|\mathbf{r}|^2}{t}\right) \\ &= A \left( \frac{b^2}{6t^{3/2}} \left( -\frac{6B}{t} + \frac{4B^2|\mathbf{r}|^2}{t^2} \right) + \frac{3}{2t^{5/2}} - \frac{B|\mathbf{r}|^2}{t^{7/2}} \right) \exp\left(-\frac{B|\mathbf{r}|^2}{t}\right) \\ &= A \left( \frac{1}{t^{5/2}} \left( -Bb^2 + \frac{3}{2} \right) + \frac{B|\mathbf{r}|^2}{t^{7/2}} \left( \frac{4b^2B}{6} - 1 \right) \right) \exp\left(-\frac{B|\mathbf{r}|^2}{t}\right) \end{aligned}$$

So  $\mathcal{L}G(\mathbf{r}, t) = 0$  if:

$$\begin{aligned} Bb^2 &= \frac{3}{2} \implies B = \frac{3}{2b^2} \\ \implies \frac{4b^2B}{6} - 1 &= \frac{6}{6} - 1 = 0 \quad \checkmark \end{aligned}$$

Hence the solution is:

$$f(\mathbf{r}, t) = \int_{all\ space} \frac{A}{t^{3/2}} \exp\left(-\frac{3|\mathbf{r} - \mathbf{r}'|^2}{2b^2t}\right) f(\mathbf{r}', 0) d\mathbf{r}'$$

The normalization constant  $A$  is set by the fact that if  $f(\mathbf{r}, 0)$  is constant in space (and  $t$  is small) then by the differential equation;

$$\frac{b^2}{6} \nabla^2 f(\mathbf{r}, t)|_{t=0} = \frac{b^2}{6} \nabla^2 f(\mathbf{r}, 0) = 0 = \frac{\partial}{\partial t} f(\mathbf{r}, t)|_{t=0} \implies f(\mathbf{r}, t) = f(\mathbf{r}, 0)$$

so  $f(\mathbf{r}, t)$  is constant in space (so just  $\mathbf{r} = 0$  can be considered) and:

$$\begin{aligned}
 f(\mathbf{r}, t) &= \int_{all\space} \frac{A}{t^{3/2}} \exp\left(-\frac{3|\mathbf{r} - \mathbf{r}'|^2}{2b^2 t}\right) f(\mathbf{r}', 0) d\mathbf{r}' \\
 &= f(\mathbf{r}, 0) \frac{A}{t^{3/2}} \int \exp\left(-\frac{3|\mathbf{r}'|^2}{2b^2 t}\right) d\mathbf{r}' \\
 &= f(\mathbf{r}, 0) \frac{A}{t^{3/2}} \int_0^\infty (r')^2 \exp\left(-\frac{3(r')^2}{2b^2 t}\right) dr' \int_0^\pi \int_0^{2\pi} \sin \theta d\theta d\phi \\
 &= f(\mathbf{r}, 0) A \pi \sqrt{\pi} \left(\frac{3}{2b^2}\right)^{-3/2} \\
 \implies A &= \left(\frac{3}{2\pi b^2}\right)^{3/2}
 \end{aligned}$$

So choosing  $t = \delta s$  and starting at any point  $s$ :

$$f(\mathbf{r}, s + \delta s) = \exp\left(\delta s \frac{b^2}{6} \nabla^2\right) f(\mathbf{r}, s) = \left(\frac{3}{2\pi\delta s b^2}\right)^{3/2} \int \exp\left(-\frac{3|\mathbf{r} - \mathbf{r}'|^2}{2b^2 \delta s}\right) f(\mathbf{r}', s) d\mathbf{r}'$$

### 7.2.4 Final solution

So the solution of the full propagator equation is:

$$\begin{aligned}
 q(\mathbf{r}, s + \delta s) &= \gamma \exp\left(\delta s \frac{b^2}{6} \nabla^2\right) q(\mathbf{r}, s) \\
 \text{where } \gamma &= \exp\left(-\delta s \exp\left(\frac{\delta s}{2} \frac{b^2}{6} \nabla^2\right) w(\mathbf{r})\right)
 \end{aligned}$$

and where the exponential is calculated through:

$$\exp\left(\delta s \frac{b^2}{6} \nabla^2\right) q(\mathbf{r}, s) = \left(\frac{3}{2\pi\delta s b^2}\right)^{3/2} \int \exp\left(-\frac{3|\mathbf{r} - \mathbf{r}'|^2}{2b^2 \delta s}\right) q(\mathbf{r}', s) d\mathbf{r}'$$

And similarly for the exponential in  $\gamma$  with  $\delta s \rightarrow \frac{\delta s}{2}$  and  $q(\mathbf{r}', s) \rightarrow w(\mathbf{r})$

# Chapter 8

## Appendix 2: Free Energy Model Calculations

### 8.1 Lens Model Calculations

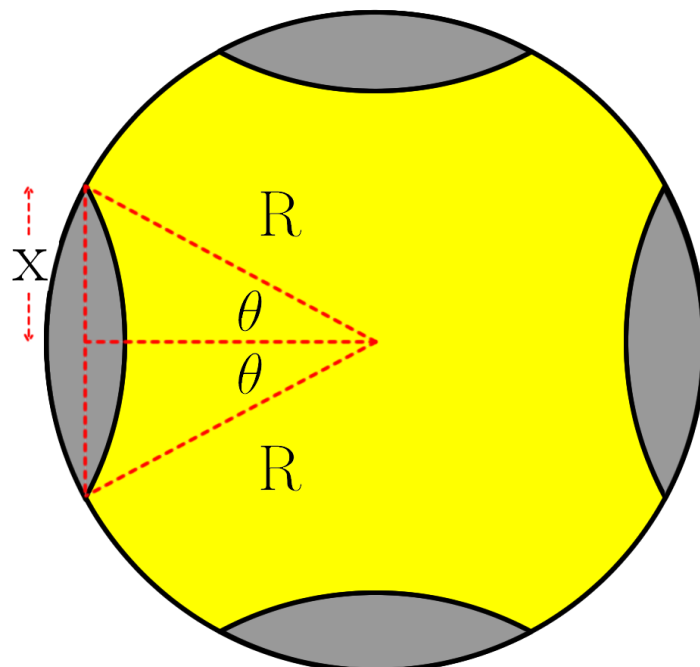


Figure 8.1: Lens model of the collapsed polymer. The yellow region is that of polymer species **B**, species **A** forms  $k$  lenses on the surface

### 8.1.1 Surface tension

The surface area and volume of each lens is found by using the solid angle of the cone  $\Omega = 2\pi(1 - \cos \theta)$ . The surface area of one side of the lens is given by:

$$\begin{aligned} A_{\frac{1}{2}\text{Lens}} &= 4\pi R^2 \frac{\Omega}{4\pi} \\ &= 2\pi R^2 (1 - \cos \theta) \\ &= 2\pi R^2 \left( 1 - \sqrt{1 - \frac{x^2}{R^2}} \right) \end{aligned}$$

Using the **A-B** surface tension equation (3.1) the free energy (in units of  $kT$ ) resulting from surface tension between species **A** and **B** of one lens is:

$$\begin{aligned} F_{AB}(\text{Lens}) &= \frac{3}{4\pi\sqrt{6}} \chi_{AB}^{1/2} \phi \frac{A_{\frac{1}{2}\text{Lens}}}{b^2} \\ &= \frac{3}{2\sqrt{6}} \chi_{AB}^{1/2} \phi \left( 1 - \sqrt{1 - \frac{x^2}{R^2}} \right) \frac{R^2}{b^2} \end{aligned}$$

Hence the total free energy resulting from **A-B** surface tension is given by:

$$F_{AB} = \frac{3}{2\sqrt{6}} \chi_{AB}^{1/2} k \phi \left( 1 - \sqrt{1 - \frac{x^2}{R^2}} \right) \frac{R^2}{b^2}$$

### 8.1.2 Species B stretching

#### Cone Stretching equation

The free energy resulting from stretching an ideal chain into a cone-shaped volume can be evaluated by generalizing the linear chain stretching energy given in the theory section Eq. (2.2). The cone is split into discs of infinitesimal height  $dz$  and radius  $R_c(N)$ , each containing  $dN'$  monomers where  $N'$  is the monomer number starting at the base of the cone. By conservation of density:

$$\begin{aligned} \phi \pi [R_c(N')]^2 dr &= \frac{4}{3} b^3 dN' \\ \implies dr &= \frac{4b^3 dN'}{\phi [R_c(N')]^2} \end{aligned}$$

The linear stretching equation applies in each infinitesimal disc:

$$\begin{aligned} dF_S &= \frac{3dr^2}{2dN'b^2} \\ &= \frac{8b^4}{3\phi^2[R_c(N')]^4} dN' \end{aligned}$$

Hence integrating over the whole half **B** block of total monomers  $N_{\frac{1}{2}\mathbf{B}}$ :

$$F_{S \text{ cone}} = \frac{8b^4}{3\phi^2} \int_0^{N_{\frac{1}{2}\mathbf{B}}} [R_c(N')]^{-4} dN' \quad (8.1)$$

This gives the stretching free energy penalty for stretching into a cone.

### B stretching

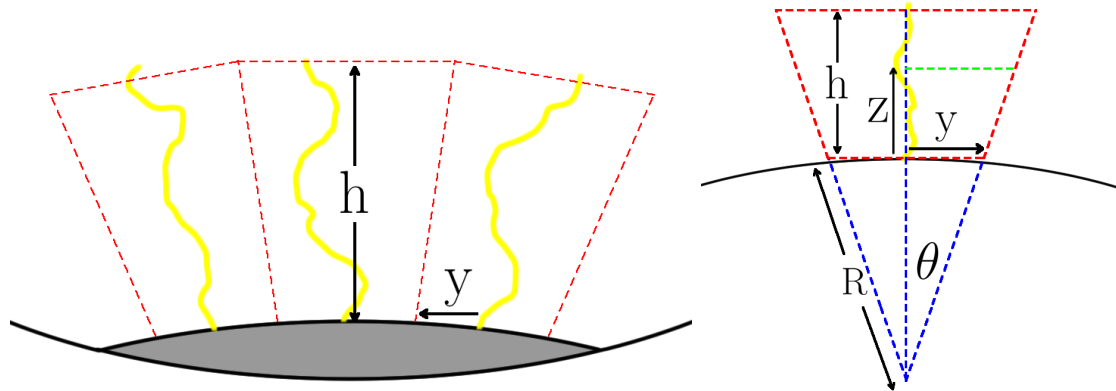


Figure 8.2: Species **B** stretching model

The expansion rate of the cone is described by the function  $r(z)$  where  $z$  is the height above the lens surface along the axis of the cone. The initial radius  $r(0) = y$  is set by the requirement that the half lens surface area be taken up by the species **B** stretching cone bases. Given that the polymer has  $n$  total blocks, then the total junction points is also  $n$  and the junction points per lens is  $\frac{n}{k}$ . Hence:

$$A_{\text{cone base}} = \frac{A_{\frac{1}{2}\text{Lens}}}{\text{jn. points}}$$

$$\Rightarrow \pi y^2 = \frac{2\pi R^2 \left(1 - \sqrt{1 - \frac{x^2}{R^2}}\right)}{n/k}$$

so:

$$y = R \sqrt{\frac{2k}{n} \left(1 - \sqrt{1 - \frac{x^2}{R^2}}\right)}$$

The function  $r(z)$  is given by:

$$\begin{aligned}\sin \theta &= \frac{r(z)}{R+z} \\ \implies r(z) &= (R+z) \sin \theta = (R+z) \frac{y}{R}\end{aligned}$$

The height  $h$  is set by the requirement that the volume of all the stretching cones must be equal to the volume of species **B** polymer. The volume of one stretching cone is given by:

$$\begin{aligned}V_{\text{cone}} &= \frac{1}{3}\pi(r(h))^2(h+R) - \frac{1}{3}\pi y^2 R \\ &= \frac{1}{3}\pi y^2 \left( \frac{(R+h)^3}{R^2} - R \right)\end{aligned}$$

Given that there are  $n$  half blocks of species **B** and there are  $N_B$  total species **B** monomers:

$$\begin{aligned}n\phi V_{\text{cone}} &= \frac{4}{3}\pi b^3 N_B \\ \implies \frac{(R+h)^3}{R^2} - R &= \frac{4b^3 N_B}{n\phi y^2}\end{aligned}$$

Hence:

$$h = R \left( \left( \frac{4b^3 N_B}{n\phi y^2 R} + 1 \right)^{1/3} - 1 \right)$$

Now to use the cone stretching equation (8.1),  $R_c(N')$  is needed. Given that each species **B** half block contains  $\frac{N_B}{n}$  monomers and assuming a linear increase of  $N'$  with  $z$ :

$$z(N') = \frac{hn}{N_B} N'$$

since then  $z(\frac{N_B}{n}) = h$ . This gives:

$$R_c(N') = r(z(N')) = (R + \frac{hn}{N_B} N') \frac{y}{R}$$

Hence by equation (8.1) the stretching free energy (in units of  $kT$ ) for each half

block in species **B** is given by the integral:

$$\begin{aligned}
 F_S(\frac{1}{2}A \text{ block}) &= \frac{8b^4}{3\phi^2} \int_0^{\frac{N_B}{n}} (R_c(N'))^{-4} dN' \\
 &= \frac{8b^4 R^4}{3\phi^2 y^4} \int_0^{\frac{N_B}{n}} \left( R + \frac{hn}{N_B} N' \right)^{-4} dN' \\
 &= \frac{8b^4 R^4}{3\phi^2 y^4} \left[ -\frac{N_B}{3hn(R + \frac{hn}{N_B} N')^3} \right]_0^{\frac{N_B}{n}} \\
 &= \frac{8b^4 N_B R^4}{9hn\phi^2 y^4} (R^{-3} - (R + h)^{-3})
 \end{aligned}$$

So the total stretching free energy due to species **B** is:

$$F_{S\mathbf{B}} = \frac{8b^4 N_B R^4}{9hn\phi^2 y^4} (R^{-3} - (R + h)^{-3})$$

### 8.1.3 Species A stretching

The base radius of each cylinder is simply given by the base radius of the corresponding species **B** stretching cone  $y$ . If the height of each cylinder is  $H$  then by conservation of volume in species **A**:

$$\begin{aligned}
 n\phi V_{\frac{1}{2} \text{ block cylinder}} &= \frac{4}{3}\pi b^3 N_A \\
 \implies \pi y^2 H &= \frac{4\pi b^3 N_A}{3n\phi} \\
 \implies H &= \frac{4b^3 N_A}{3n\phi y^2}
 \end{aligned}$$

Hence by the linear stretching equation (2.2) the stretching free energy in each cylinder is:

$$\begin{aligned}
 F_S(\frac{1}{2} \text{ block cylinder}) &= \frac{3H^2}{2N_C b^2} \\
 &= \frac{3n}{2N_A b^2} \frac{16b^6 N_A^2}{9n^2 \phi^2 y^4} \\
 &= \frac{8b^4 N_A}{3n\phi^2 y^4}
 \end{aligned}$$

so the total stretching free energy due to species **A** is:

$$F_{S\mathbf{A}} = \frac{8b^4 N_A}{3\phi^2 y^4}$$

### 8.1.4 Relating $k$ to $x$

The volume of one lens is:

$$\begin{aligned} V_{\text{Lens}} &= 2(V_{\text{cap}} + V_{\text{cone}} - V_{\text{cone}}) \\ &= 2 \left( \frac{4}{3}\pi R^3 \frac{\Omega}{4\pi} - \frac{1}{3}\pi x^2 \sqrt{R^2 - x^2} \right) \\ &= 2 \left( \frac{2}{3}\pi R^3 \left( 1 - \sqrt{1 - \frac{x^2}{R^2}} \right) - \frac{1}{3}\pi x^2 R \sqrt{1 - \frac{x^2}{R^2}} \right) \\ &= \frac{4}{3}\pi R^3 \left( 1 - \sqrt{1 - \frac{x^2}{R^2}} \left( 1 + \frac{x^2}{2R^2} \right) \right) \end{aligned}$$

Given that species **A** consists of  $N_A$  monomers at a constant volume fraction  $\phi$ :

$$\begin{aligned} k\phi V_{\text{Lens}} &= \frac{4}{3}\pi b^3 N_A \\ \Rightarrow \quad \frac{k\phi R^3}{b^3 N_A} &= \left( 1 - \sqrt{1 - \frac{x^2}{R^2}} \left( 1 + \frac{x^2}{2R^2} \right) \right)^{-1} \end{aligned}$$

Hence using the volume fraction equation (2.4) an equation that relates the number of lenses  $k$  to the size of each lens  $x$  is obtained:

$$\frac{N_A}{kN} = 1 - \sqrt{1 - \frac{x^2}{R^2}} \left( 1 + \frac{x^2}{2R^2} \right)$$

## 8.2 Micelle Model Calculations

### 8.2.1 Surface tension

This system is significantly simpler to model as species **A** is simply a sphere in the middle of the larger sphere of species **B**. The **A-B** surface tension free energy is given by (equation (3.1)):

$$\begin{aligned} F_{AB} &= \frac{3}{4\pi\sqrt{6}} \chi_{AB}^{1/2} \phi \frac{A_{\mathbf{A} \text{ sphere}}}{b^2} \\ &= \frac{3}{\sqrt{6}} \chi_{AB}^{1/2} \phi \frac{R_{\mathbf{A} \text{sphere}}^2}{b^2} \end{aligned}$$

So using equation (2.4) for the species **A** sphere:

$$F_{AB} = \frac{3}{\sqrt{6}} \chi_{AB}^{1/2} \phi^{1/3} N_A^{2/3}$$

### 8.2.2 Species B stretching

Using the same cone as in figure 8.2 the base radius  $y$  is set by dividing up the sphere surface area into  $n$  circles corresponding to each junction point:

$$\begin{aligned} n\pi y^2 &= 4\pi R_A^2 \\ \implies y &= \frac{2R_A}{\sqrt{n}} \end{aligned}$$

This then gives:

$$\begin{aligned} \frac{y}{R_A} &= \sin \theta = \frac{r(z)}{R_A + z} \\ \implies r(z) &= \frac{2}{\sqrt{n}}(R_A + z) \end{aligned}$$

By conservation of volume in species **B**:

$$\begin{aligned} n(V_{\text{cone } h+R} - V_{\text{cone } R}) &= \frac{4}{3}\pi b^3 N_B \\ \implies \frac{n\pi}{3} ((r(h))^2 (R_A + h) - y^2 R_A) &= \frac{4}{3}\pi b^3 N_B \\ \implies n \left( \frac{4(R_A + h)^3}{n} - \frac{4R_A^3}{n} \right) &= 4b^3 N_B \\ \implies h &= R_A \left( \left( \frac{b^3 N_B}{R_A^3} + 1 \right)^{1/3} - 1 \right) \end{aligned}$$

Again, the function  $z(N') = \frac{hn}{N_B} N'$  so

$$r(N') = \frac{2}{\sqrt{n}}(R_A + \frac{hn}{N_B} N')$$

Using the cone stretching equation (8.1):

$$\begin{aligned} F_{S\mathbf{B}} &= \frac{8b^4}{3\phi^2} \int_0^{\frac{N_B}{n}} \frac{n^2}{4} \left( R_A + \frac{hn}{N_B} N' \right)^{-4} dN' \\ &= \frac{2b^4 n^2}{3\phi^2} \left[ -\frac{N_B}{3hn(R_A + \frac{hn}{N_B} N')^3} \right]_0^{\frac{N_B}{n}} \\ &= \frac{2b^4 n N_B}{9\phi^2 h} (R_A^{-3} - (R_A + h)^{-3}) \end{aligned}$$

so the stretching in species **B** gives free energy:

$$F_{S\mathbf{B}} = \frac{2b^4 n N_B}{9\phi^2 h R_A^3} \left( 1 - \left( 1 + \frac{h}{R_A} \right)^{-3} \right)$$